AD-A267 479 REMOTE SENSING OF PRECIPITATION AND ELECTRIFICATION WITH A DUAL-POLARIZAT..(U) NEW MEXICO INST OF MINING AND TECHNOLOGY SOCORRO GEOPHYSICAL.. P KREHBIEL ET AL. 171

UNCLASSIFIED 10 JUL 93 AFOSR-TR-93-0564 AFOSR-89-0450 NL

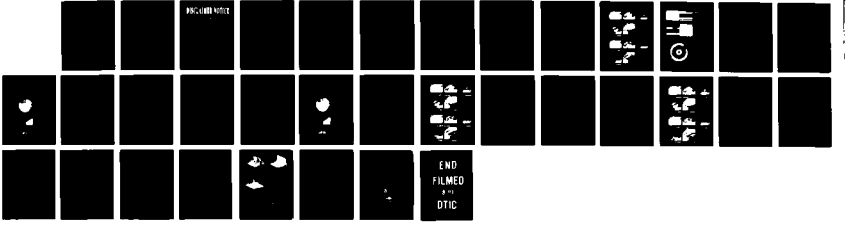

SECURITY CLASSIFICATION OF THIS PAGE

AD-A267 479

REI

1a. REPORT SECURITY CLASSIFICATION
UNCLASSIFIED

2a. SECURITY CLASSIFICATION AUTHORITY

2b. DECLASSIFICATION / DOWNGRADING SCHEDULE

DTIC ELECTE AUG 4 1993 S C D

3. DISTRIBUTION / AVAILABILITY OF REPORT
Approved for public release; distribution is unlimited.

4. PERFORMING ORGANIZATION REPORT NUMBER(S)

5. MONITORING ORGANIZATION REPORT NUMBER(S)

6a. NAME OF PERFORMING ORGANIZATION	6b. OFFICE SYMBOL (If applicable)	7a. NAME OF MONITORING ORGANIZATION
New Mexico Institute of Mining and Technology		AFOSR/NL

6c. ADDRESS (City, State, and ZIP Code)	7b. ADDRESS (City, State, and ZIP Code)
Geophysical Research Center Campus Station Socorro, NM 87801.	Building 410 Bolling AFB, DC 20332-6448

8a. NAME OF FUNDING / SPONSORING ORGANIZATION	8b. OFFICE SYMBOL (If applicable)	9. PROCUREMENT INSTRUMENT IDENTIFICATION NUMBER
AFOSR	NL	AFOSR-89-0450

8c. ADDRESS (City, State, and ZIP Code)	10. SOURCE OF FUNDING NUMBERS			
	PROGRAM ELEMENT NO.	PROJECT NO.	TASK NO	WORK UNIT ACCESSION NO.
Building 410 Bolling AFB, DC 20332-6448	61102F	2310	A1	

11. TITLE (Include Security Classification)
Final Report for AFOSR Grant AFOSR-89-0450, "Remote Sensing of Precipitation and Electrification with a Dual-Polarization Coherent/Wideband Radar"

12. PERSONAL AUTHOR(S)
Paul Krehbiel and Grant Gray

13a. TYPE OF REPORT	13b. TIME COVERED	14. DATE OF REPORT (Year, Month, Day)	15. PAGE COUNT
Final	FROM 89-07-15 TO 93-07-14	10 July 1993	29

16. SUPPLEMENTARY NOTATION

17. COSATI CODES			18. SUBJECT TERMS (Continue on reverse if necessary and identify by block number)
FIELD	GROUP	SUB-GROUP	

19. ABSTRACT (Continue on reverse if necessary and identify by block number)

Electrical alignment of precipitation particles was detected in an electrified storm using the co- and cross-polar channels of the radar. The radar receiver chain was upgraded and modern signal processing and display equipment added. The system was taken to Kennedy Space Center for final checkout and data-gathering independently and in conjunction with the CaPE program. Using the cross-polar correlation magnitude and phase displays as a guide, it was possible to accurately predict the outset of electrification and attendant lightning discharges, and to determine when a storm would no longer produce lightning. Several publications documenting the effect are included. A patent on the cross-polar correlation technique is being sought.

93-17441

20. DISTRIBUTION / AVAILABILITY OF ABSTRACT	21. ABSTRACT SECURITY CLASSIFICATION
☐ UNCLASSIFIED/UNLIMITED ☒ SAME AS RPT. ☐ DTIC USERS	UNCLASSIFIED

22a. NAME OF RESPONSIBLE INDIVIDUAL	22b. TELEPHONE (Include Area Code)	22c. OFFICE SYMBOL
Maj James Kroll	(202) 767-5021	NL

DD FORM 1473, 84 MAR — 83 APR edition may be used until exhausted. All other editions are obsolete.

SECURITY CLASSIFICATION OF THIS PAGE

☆ U.S. Government Printing Office: 1988—607-044

DISCLAIMER NOTICE

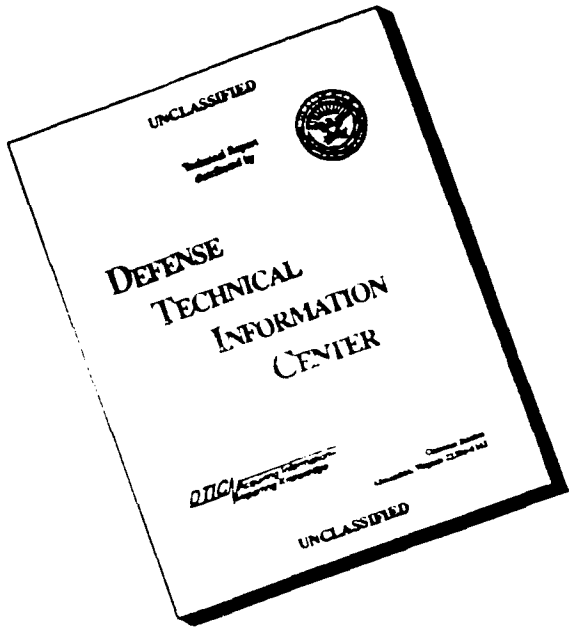

THIS DOCUMENT IS BEST QUALITY AVAILABLE. THE COPY FURNISHED TO DTIC CONTAINED A SIGNIFICANT NUMBER OF PAGES WHICH DO NOT REPRODUCE LEGIBLY.

Final Report for AFOSR Grant AFOSR-89-0450
"Remote Sensing of Precipitation and Electrification with a
Dual-Polarization, Coherent, Wideband Radar System"
July 15, 1989 to July 15, 1993

The first year's research provided solid evidence of the capability of dual-polarization radar to detect extensive regions of particle alignment in electrified clouds. As was anticipated in the proposal, we were able to verify that lightning echoes are detectable by 3 cm. radar by observing the cross-polar return. A more detailed description is included in the "First Year Interim Report – Grant # AFOSR-89-0450", and in Krehbiel, et al, 1991 (attached).

On the basis of the first year's results, during the second year of the contract extensive upgrades to the receiver chain for the radar were made. Real-time signal processing and display systems were added to the system to supplement the existing time-series recording system, and to give the radar operator(s) timely operational information so as to better manage radar resources during an experiment. Completion of the modifications was targeted for June, 1991, so that the system could participate in the Convective and Precipitation Experiment (CaPE) at Kennedy Space Center, Florida, during July/August of 1991.

Modification to the radar receiver were focussed primarily on the intermediate frequency (IF) section where critical analog pre- processing is performed. An IF switching network was installed so that the co- and cross-polar channels are each processed through their own IF chain rather than alternating with the transmitted polarization. This modification significantly improved measurement accuracy and allows setting higher gain for the weaker cross-polar returns. Filters were placed at critical points in the IF chain to improve rejection of unwanted signals. A modern set of analog drivers was installed to allow electronic selection of the data sources for the A/D converters.

A real-time Digital Signal Processor (DSP) system was added to the existing analog-to-digital (A/D) converter/digital instrumentation recorder scheme in such a way that the data source for the signal processor could be switched transparently between the direct A/D output and previously recorded A/D data from the recorder. A serial housekeeping data stream with antenna angles, time, and other pertinent data was recorded as well. The signal processor cards themselves are off-the-shelf units from Ariel Corp. and employ the Motorola DSP56000 DSP chip. Each card is capable of a peak computational rate of 27 million multiply/accumulate (MAC) operations per second. The system currently requires two such DSP cards.

The DSP cards plug directly into a PC/AT-style computer. A 33 MHz 386 computer was chosen as the host, as it was the fastest available PC style machine at the time of ordering. The host was equipped with 8 megabytes of 0 wait-state memory, an Ethernet card for communication with other systems (SUN IPC's, in particular), and a Super-VGA video card capable of producing 800 x 600 point display resolution in 256 colors. A 500 Megabyte fast hard disk subsystem was added for preliminary data recording.

During non-operational times data from the PC/AT disk are transmitted over Ethernet to the SUN IPC's 1 gigabyte disk and then archived onto Digital Audio Tapes (DATs). DSP software was written to compute, in real-time, mean co-polar and cross-polar signal power (P_{hh} and P_{hv}), differential reflectivity (Z_{dr}), linear (or circular) depolarization ratio (LDR/CDR), Doppler velocity ($\overline{V}$), cross-polar correlation amplitude and phase (ρ_x and ϕ_x).

The radar system was shipped via rail to Kennedy Space Center, Florida, on July 15, 1991. Our objectives for the KSC effort were to a) complete and test the upgraded radar and the real-time processing/display system, b) follow up on the work done by Hendry and McCormick on particle alignment in electrified storms, and c) to participate in CaPE Project operations. Hendry and McCormick had suggested that the correlation coefficient between the co- and cross-polar received signals could be used to identify regions of strongly aligned cloud partices. Of particular interest were regions above the freezing level where ice particles align with a strong electric field.

Prior to shipping the radar Paul Krehbiel and Grant Gray had visited KSC and had picked a site near the Shuttle Landing Facility (SLF) for the NM Tech radar operations. The site was near a 5 cm tracking radar operated for NASA by Lockheed. The NCAR CP2 radar was located 18 km NNW of the Tech radar and in good position for coordinated multipolarization studies and dual Doppler measurements. The NM Tech radar was in place July 29 and ready for initial testing.

During setup a coolant line fault resulted in damage to the transmitter final amplifier tube. The manufacturer, Hughes Microwave Division, quickly repaired the tube and returned it to us at KSC. In the meantime we continued work on the DSP and display software. The radar was back in operation on 17 August.

After over two weeks of dry weather, we finally observed some precipitation echos, but with little apparent associated electrical activity. Toward mid-September we were fortunate to begin seeing cases of strongly electrified storms within radar range. On September 15, after working out some bugs in the correlation code, we saw our first electrification signature. High values of cross-polar correlation above the freezing level were observed, as predicted. Though we expected to see decreases in correlation following lightning discharges, we were surprised that the effect would be so dramatically apparent on the color-enhanced radar display. This afforded solid evidence not only that the description of the alignment effect was accurate, but that the radar was working quite well, with excellent isolation between the orthogonal polarizations.

Using the correlation magnitude and phase displays, NM Tech radar operators and visitors alike quickly became skilled at predicting the time and place of lightning strikes. KSC personnel expressed interest in the technique as a means to reduce delays incurred in transporting electrostatic-sensitive rocket components between sites during electrical storms. In addition, the correlation technique offers the capability of more accurately evaluating lightning hazards posed to launch operations.

With the radar operating in circular polarization mode we were able to use the phase of

the complex cross-polar correlation to determine changes in the angle of orientation of ice particles. In many instances we observed slow shifts in phase leading up to a discharge, with sudden large phase shifts immediately following the discharge, indicating rotation of the particles with the electric field changes. In many cases, change in correlation phase was as dramatic an indicator of elecrification condition as was the correlation amplitude change. The alignment was also observable when operating in linear polarization, but was not as dramatic. Since the correlation is performed between the co- and cross-polar returns it is possible to have nulls in the correlation computation when particles are aligned with, or are normal to, the incident polarization, since the cross-polar return is extremely small in those cases. This does not occur for circular polarization. Circular polarization is the preferred mode for implementing this technique.

The CaPE project terminated operations on August 19, but plans had been made by NM Tech to continue independent measurements and to make coordinated measurements with NCAR's CP2 between August 19 and October 1. Several cases of dual Doppler and tomographic data (storms directly between the the NM Tech and CP2 radars) were recorded during the period from 19 August to 1 October.

Following shutdown of CP2 operations, two days were spent acquiring both raw and processed sea clutter data. The NM Tech radar was disassembled and readied for rail shipment back to Socorro during October 6-10.

Upon returning to Socorro, Gray and Chen began writing software for radar data perusal, cataloging, and analysis. Krehbiel, Gray, Rison, and Chen prepared and delivered a presentation on the cross-polar correlation technique at the *1991 Fall AGU meeting* in San Francisco. In June, 1992, Krehbiel delivered a presentation to the Ninth International Conference on Atmospheric Electricity in St. Petersburg, Russia. Also in June, Blackman presented results at the URSI Commision F Open Symposium at Ravenscar, UK.

The radar finally returned by rail in late December. During January '92 it was reassembled in the NM Tech Workman Center compound. The cooling system was purged and safety pressure releases were installed at critical points to ensure that the overpressure and consequent near disaster experienced at KSC could not recur. The radar transmitter's aging grid modulator had become unreliable. McCrary and Gray designed and constructed a smaller, more robust replacement using modern components. During June and early July of 1992, the radar was prepared to gather data coordinated with the Langmuir Lab lightning studies later in the summer. Though not a particularly active summer, electrically speaking, some data were recorded in order to verify the proper operation of the new modulator circuit. The correlation magnitude and phase effects were observed in conjunction with lightning events in these arid climate thunderstorms, as well. McCrary modified the radar trailer air conditioning controls to provide more even temperature regulation. The 500 megabyte data recording disk in the radar data acquisition computer failed in January, 1993, and a new unit has been ordered.

Efforts since last summer have centered primarily around analysis of data and reporting of results. Application has been made for a US patent on the correlation technique.

Several AN/APQ-130 16 GHz radars were obtained as excess property from Cannon AFB at Clovis, NM. These were removed from F-111D fighter aircraft which are being decommissioned. We are studying the possibiliy of converting one or more of these units into highly portable Doppler/electrification radars.

Graduate Students: Support for one graduate student, Tiehan Chen, was provided by the grant. Mr. Chen designed hardware and software for the data acquisition and display system, including assembly language for the signal processors. He is now engaged in detailed analyses of selected storm cases for preparation of his doctoral dissertation.

Radar Scientist/Engineer: Mr. Grant Gray, a radar signal processing specialist formerly at the National Center for Atmospheric Research in Boulder, Colorado, was hired as a full-time project engineer starting 1 July, 1991.

Publications/Presentations: The following publication and presentations have resulted from the work on this grant:

Krehbiel, P., T. Chen, S. McCrary, W. Rison, G. Gray, M. Brook: Dual Polarization Radar Indications of the Potential for Lightning in Storms Near Kennedy Space Center, Florida. *Preprints; 26th International Conference on Radar Meteorology.* AMS. Norman, May, 1993.

Rison, W., G. Gray, P. Krehbiel, T. Chen: A Compact, Real-time Radar Signal Processing and Display System. *Preprints; 26th International Conference on Radar Meteorology.* AMS. Norman, May, 1993.

Gray, G. R., W. Rison, P. Krehbiel, T. Chen: A PC-Based Real-Time Signal Processing and Display System. *Preprints: 8the Symposium on Meteorological Observations and Instrumentation.* AMS, Anaheim, CA, Jan., 1993.

Krehbiel, P., T. Chen, S. McCrary, W. Rison, G. Gray, T. Blackman, M. Brook. Presentation: American Geophysical Union, Fall Meeting. San Francisco. December, 1991.

Krehbiel, P., T. Chen, S. McCrary, W. Rison, G. Gray, T. Blackman, M. Brook. Dual-Polarization Radar Signatures of the Potential for Lightning in Electrified Storms. *Proceedings: Ninth International Conf. on Atmospheric Electricity.* St. Petersburg, Russia. June, 1992.

Krehbiel, P., T. Chen, S. McCrary, W. Rison, G. Gray, T. Blackman, M. Brook. Lightning Precursor Signatures from Dual-polarization Radar Measurements of Storms. *Proceedings: URSI Commission F Open Symposium.* Ravenscar, UK. June, 1992.

Rison, W., P. Krehbiel, T. Chen, and P, Gondalia: Design of a PC-based Real-Time Radar Display. *Preprints: 25th International Conference on Radar Meteorology,* AMS. Paris, June 1991. pp 227-228.

Krehbiel, P., W. Rison, S. McCrary, T. Blackman: Dual Polarization Observations of Lighting Echoes and Precipitation Alignment at 3 cm Wavelength, *Preprints; 25th International Conference on Radar Meteorology,* AMS. Paris, June 1991. pp 901-904.

Copies of the above papers and abstracts are attached.

In addition, a Letter has been prepared for submission to Nature Magazine, London, entitled:

Krehbiel, P. R., T. Chen, S. McCrary, W. Rison, G. R. Gray, M. Brook: Lightning Precursor Signature from Radar Observations of Storms.

26th International Conference on Radar Meteorology
May 24-28, 1993; Norman, Oklahoma

Dual-Polarization Radar Indications of the Potential for Lightning in Storms near Kennedy Space Center, Florida

Paul Krehbiel, Tiehan Chen, Stephen McCrary, William Rison, Grant Gray, Marx Brook

Langmuir Laboratory, Geophysical Research Center
New Mexico Tech, Socorro, NM 87801

1. Introduction. Following up on the pioneering studies of Hendry and McCormick (1976), dual-polarization radar observations of electrified storms have provided dramatic indications of the buildup of the electric field between lightning discharges and of the sudden collapse of the field at the time of lightning. The indications have been obtained by coherently correlating the co-polar and cross-polar returns from the storm, in real time using a PC-based digital signal processor. The simultaneous co- and cross-polar signals are correlated in the same manner as mean Doppler signals to determine both the squared magnitude $|\rho|^2$ and phase ϕ of the complex correlation function. The observations were obtained during the CaPE program at Kennedy Space Center, Florida in 1991 using the New Mexico Tech dual-polarization radar.

2. Observations and Results. Figure 1 shows vertical cross-sections of the various polarization variables from two sequential scans of a storm on Day 278, 1991. Figure 1a shows a vertical scan just before a lightning discharge. Figure 1b shows the same cross-section 20 seconds later, just after the lightning discharge. In the scan just prior to the lightning, two regions of strong correlation ($|\rho|^2 > 0.75$) existed at mid-levels (6-9 km MSL) in the far cell of the storm and in the upper levels (9-12 km) of the near cell. These were associated with local maxima in the cross-polar reflectivity and circular depolarization ratio (CDR). After the discharge, the correlation regions had disappeared and the associated cross-polar returns and CDR had diminished in intensity. The co-polar returns were unchanged in the two scans, as were the cross-polar returns and CDR values below the melting level, at 4-4.5 km altitude.

Correlation signatures such as shown above are readily identified in scanning through a storm and appear always to be present in electrified storms. As discussed by Hendry and McCormick (1976) and by Hendry and Antar (1982), the correlation signatures indicate the presence of electrically aligned particles, apparently ice crystals, which progressively depolarize the radar signal as it propagates through the region of aligned particles. The depolarization is cumulative in range and produces relatively strong returns of a cross-polar sense from non-depolarizing particles in and beyond the alignment region that are perfectly correlated with the co-polar return. The phase ϕ of the correlation provides a measure of the direction of alignment and also indicates the nature of the depolarization process.

Figure 2 shows how the polarization quantities vary with time and range when the antenna is pointed in a fixed direction through the electrically active region of a storm. The variables are the same as in Figure 1 and are displayed over a 20 second time interval. Lighting occurred partway through the interval and caused sudden decreases in $|\rho|^2$ and in the cross-polar power and CDR. The correlation phase also changed but no change was detected in the co-polar return. Figure 3 shows an example of how $|\rho|^2$ varies over a longer, two-minute time interval, again with fixed pointing. The correlation is observed to increase gradually with time between lightning discharges and to decrease suddenly at the time of lightning.

The correlation signatures have been found to provide an excellent indicator of the potential for lightning in a storm and we have used them to predict the occurrence of numerous lightning discharges. The correlation measurements have also been used to detect the initial electrification of storms and to determine when a storm is finished producing lightning. Storms which do not produce lightning exhibit weak correlation values above the 0° level. Alignment regions can be detected with linear polarization but circular polarization (as shown) produces significantly stronger correlation values because the depolarization is independent of alignment direction. As seen in Figure 2, particle alignment produces depolarization maxima aloft and therefore can also be detected by incoherent measurements (see also Krehbiel *et al.*, 1991).

3. Acknowledgments. This research was supported by the U.S. Air Force Office of Scientific Research under Grant AFOSR-89-0450.

4. References.

Hendry, A., and Y.M.M. Antar (1982): Radar observations of the polarization characteristics of lightning-induced realignment of atmospheric ice crystals. *Radio Sci.*, **17**, 1243-1250.

Hendry, A., and G.C. McCormick (1976): Radar observations of the alignment of precipitation particles by electrostatic fields in thunderstorms. *J. Geophys. Res.*, **81**, 5353-5357.

Krehbiel, P.R., W. Rison, S. McCrary, T. Blackman, and M. Brook (1991): Dual-polarization radar observations of lightning echoes and precipitation alignment at 3 cm wavelength. Preprints, 25th Conf. Radar Meteorology, Paris, Amer. Meteor. Soc., 901-904.

Figure 1a. Vertical cross-sections of *a*) co-polar reflectivity, *b*) circular depolarization ratio, *c*) cross-polar reflectivity, and the correlation quatities $|\rho|^2$ (*d*) and ϕ (*e*), just prior to a lightning discharge in the storm. The distance scale is 3 km per tic mark. Contours are at 20 dB intervals for reflectivities, 12 dB for CDR, 0.25/1.0 for $|\rho|^2$ and $\pi/2$ for ϕ.

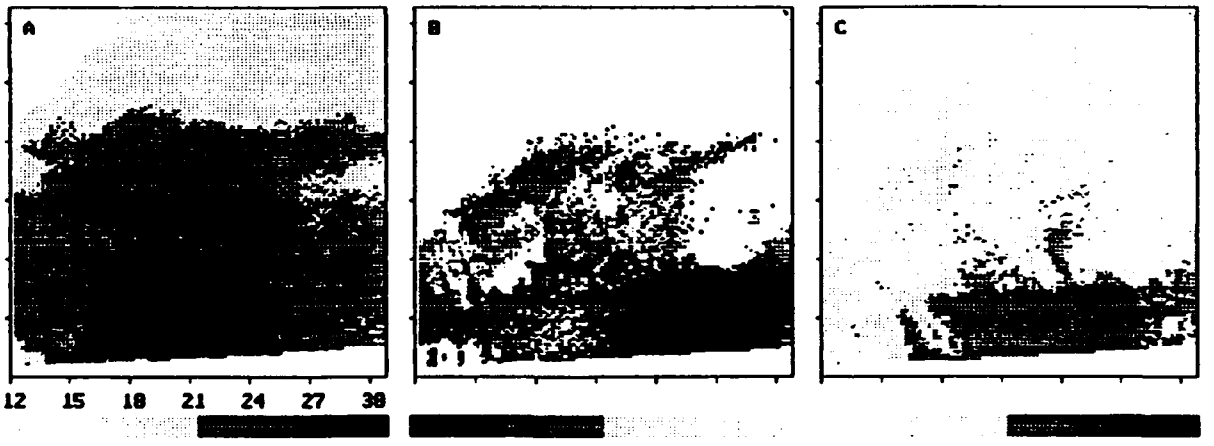

Figure 1b. Same as *Figure 1a.* except 20 seconds later, just after an intracloud discharge occurred in the storm. The electric field change of the discharge is shown above. Note disappearance of $|\rho|^2$ correlation regions.

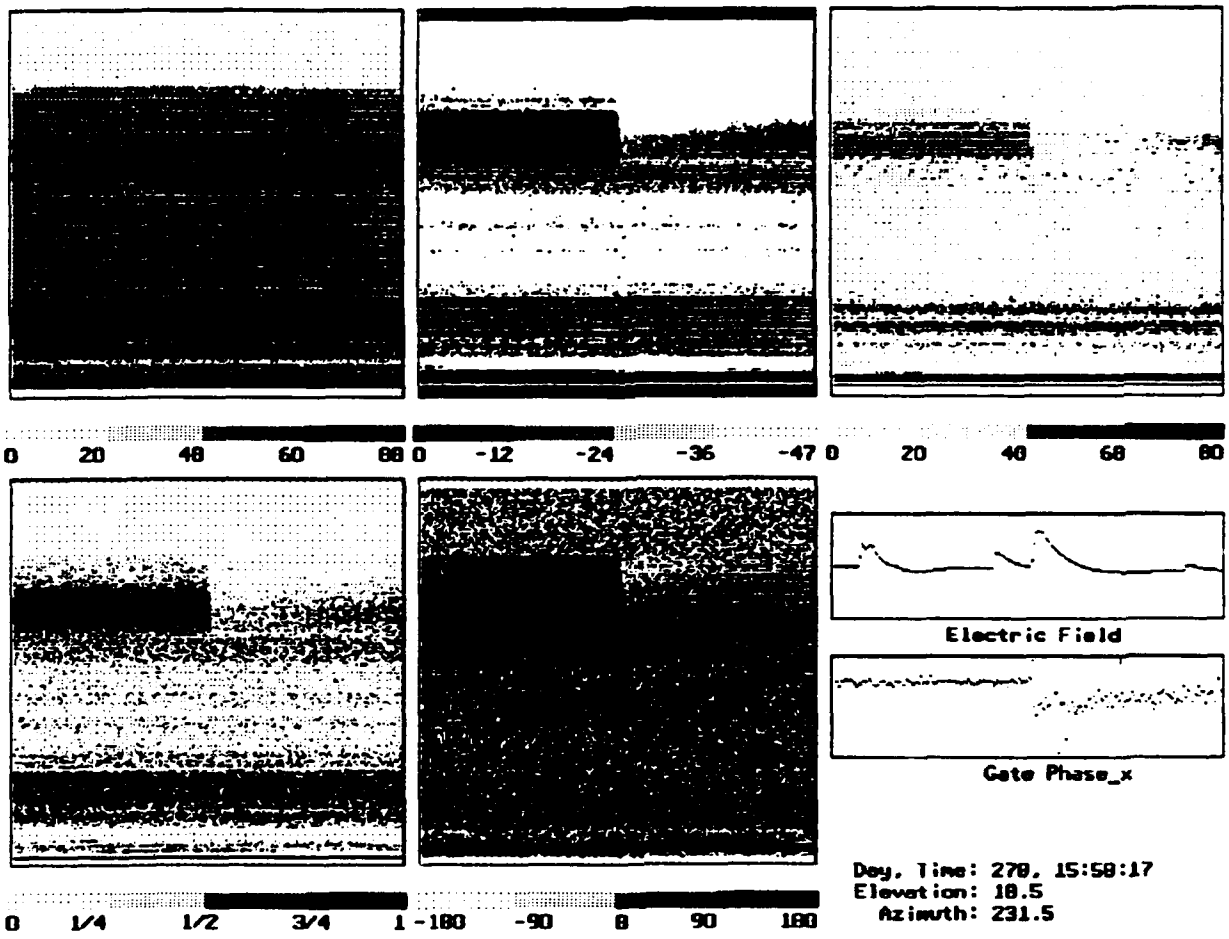

Figure 2 (above). Variation of radar signals vs. range and time for a 20 second interval around the time of lightning. Range is displayed vertically (0–37.5 km) and time increases from left to right. Panels are the same as in Figure 1. Data in the electric field panel are time-correlated with the radar observations; the first two lightning events were from other storms while the third was in the storm being observed.

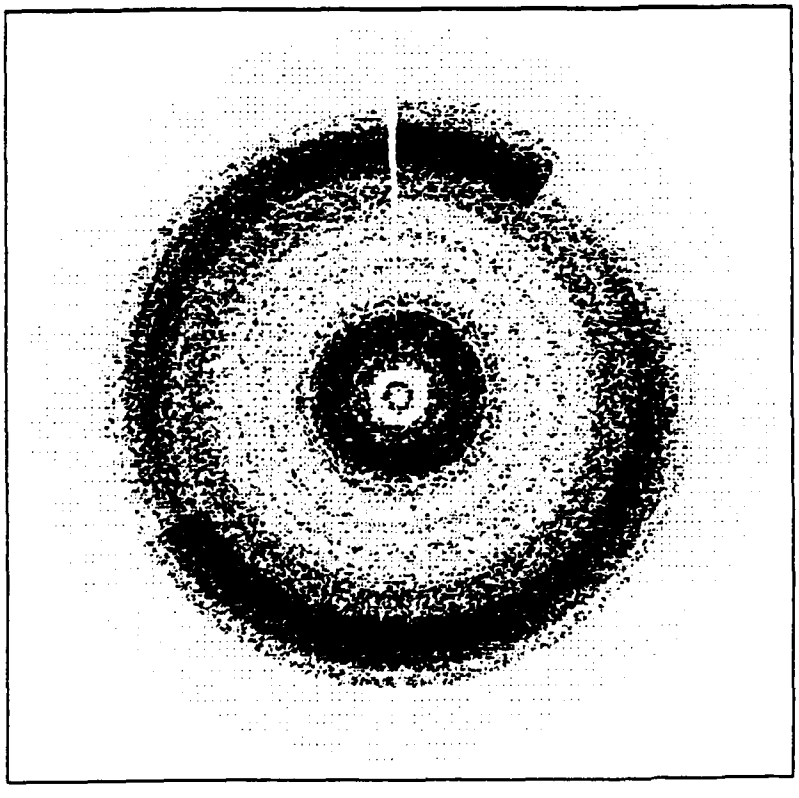

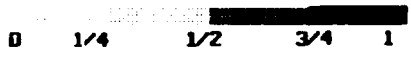

Figure 3 (left). Variation of the squared magnitude $|\rho|^2$ of the co-polar – cross-polar correlation vs. range and time over a two minute interval, showing the build-up of the correlation and particle alignment between lightning discharges. Range is displayed radially (0–37.5 km) and time increases clockwise. Elevation angle is 18.5°. Scale is above.

A COMPACT REAL-TIME RADAR SIGNAL PROCESSING AND DISPLAY SYSTEM

William Rison Grant Gray Paul R. Krehbiel
Tiehan Chen
Geophysical Research Center
New Mexico Institute of Mining and Technology,
Socorro, New Mexico 87801

1. Introduction

In 1991, we reported on a design for a small and inexpensive signal processing and display system for the New Mexico Tech Wideband, Coherent Radar [3]. The resulting system allowed us to probe and analyze various characteristics of electrified storms at Kennedy Space Center during the summer of 1991[4]. [1]

A block diagram for the processing/display system is shown in Figure 1. It consists of four major sections — the radar data stream, the hardware interface between the radar and the DSPs, the DSPs themselves, and the host computer with its display monitor. The system also incorporates an instrumentation recorder with a digital interface for recording raw time series data from the analog to digital converters.

2. The New Mexico Tech Radar

The radar is a multi-parameter 9.8 GHz system capable of transmitting 24 KW linearly or circularly polarized pulses, and simultaneously receiving both co- and cross-polar returns via a dual receiver chain. The transmitter has two modes of operation: fixed frequency and wideband noise. The fixed frequency mode is used for coherent measurements, such as Doppler velocity or complex cross-polar correlation magnitude and phase. The wideband noise mode allows accurate reflectivity estimates to be made from very few pulses and is used primarily for studies requiring high antenna scan rates and, consequently, short dwell times. These modes may be interlaced, if desired. PRF options are 2, 4, and 8 KHz. Pulse widths are selectable from 200 nsec to 1usec.

The received signals are digitized at a 1 MHz rate, for a range resolution of 150m. The azimuth, elevation, transmitted polarization, attenuation settings, time, and other auxiliary data are clocked out serially with the digitized return data. A 24 bit sync word is embedded in the serial data stream to indicate the start of each pulse. The serial housekeeping stream is also recorded on a single track of the instrumentation recorder. The interface is so designed so that the instrumentation recorder output is electrically indistiguishable from live radar data from the point of view of the DSP's.

3. Radar/DSP Interface

A minimal hardware interface buffers the data to the DSP cards. The parallel data is clocked into alternating First-In-First-Out (FIFO) buffers, so the DSPs may access data asynchronously. While one FIFO bank is being written into by the radar, the other bank is being read asynchronously by the DSPs. The FIFO banks are switched at each radar pulse.

4. DSPs

The system employs the 27 MHz Motorola 56001 DSP chip executing 13.5 Million Instructions Per Second (MIPS). The 56001 offers a 24 bit word width, a 24 bit parallel interface for data I/O, built-in hardware for serial I/O, and an 8 bit host port to communicate with a host computer. A powerful data handling feature of the 56001 is its zero-overhead interrupt mode. In our system it allows us to extract data from the

[1] This work was supported by the Air Force Office of Scientific Research under Grant # AFOSR-89-0450.

DSP without interrupting the DSP's processing operations. At present, one DSP card computes incoherent quantities such as reflectivity (Z_{hh} or Z_{vv}), cross-polar power (P_{hv}), linear/circular depolarization ratio (LDR/CDR), and differential reflectivity (Z_{dr}). The other card handles coherent parameters, including mean Doppler velocity ($\overline{v}$), or complex cross-polar amplitude (ρ_x) and phase (ϕ_x).

5. Host Computer

The 33 MHz '386 PC/AT host computer uploads code to the DSP's, controls operation of the DSP's, generates the display, and controls data archival. After the DSP's have processed a set of samples, the host is signalled via a flag register that new data are available. The host then reads and displays the data, and sends the data to the 500 Mbyte disk, if recording is enabled. After operations have terminated for the day, data are send over Ethernet to a Sun IPC and then to a Digital Audio Tape (DAT) for permanent archival.

We are using Watcom's Optimizing C Compiler for the data acquisition and display code. This produces protected mode code which executes 2-3 times as fast as in real mode. For the DSP code we are using the standard Motorola assembler/linker.

6. Display

The Super-VGA display offers 800 horizontal by 600 vertical pixels with 256 colors available for each pixel, of which 16 colors are used for data and 4 for alert conditions. A (black-and-white) depiction of the primary display is shown in Figure 2. Any of the parameters generated in the DSP may be displayed here. The 500 x 500 pixel area in the upper left defaults to a PPI presentation. The smaller 250 x 250 pixel area in the upper right defaults to RHI, but the roles of two areas may be reversed. The large area is also used in Time vs. Range format for observations at fixed antenna angles. Zooms of up to 4:1 are available and the display may be offset in any direction. Two additional rectangular plotting areas positioned below the small RHI area on the right side of the screen display a strip-chart representation of local electric field and an A-scope display of the selected parameter. Nearly all commands to the display and data acquisition functions consist of individual keystrokes on the host computer keyboard.

The alternate display, shown in Figure 3, contains five 250 x 250 rectangular areas simultaneously displaying: Z_{hh}, LDR, Z_{hv}, and either ρ_x and ϕ_x, or $\overline{v}$. An A-scope presentation of a selected parameter is include here, as well.

7. Conclusions

Excluding labor, the entire signal processing and display system cost less than $10,000 — about $5,000 for the host computer, monitor, and disk, $2,000 for the two DSP cards, $1,000 for the software, and $1,500 for parts to build the hardware interface. The 33 MHz 386 PC/AT is marginally fast enough to handle both archival and display generation, and we plan to replace it with a faster 66 MHz 486 with local bus disk and display controllers. With a suitable multitasking operating system installed, we plan to incorporate antenna controls in the host, as well.

8. References

1. Gray, G., R. Serafin, R. Reinhart, J. Boyajian, 1975: Real-time Color Display for Meteorological Radar. Preprints: *16th Conf. on Radar Meteorology.* Amer. Met. Soc., Houston.

2. Gray, G., C. Walther, R. Keeler, C. Frush, J. Vinson, 1989: A New Programmable Signal Processor for NCAR Meteorological Radars. Preprints: *24rd Conf. on Radar Meteorology.* Amer. Met. Soc., Tallahassee.

3. Rison, W., P. Krehbiel, T. Chen, P. Gondalia, 1991: Design of a PC-based Real-time Radar Display. Preprints: *25th International Conference on Radar Meteorology.* Amer. Met. Soc., Paris.

4. Krehbiel, P., T. Chen, S. McCrary, W. Rison, G. Gray, T. Blackman, M. Brook, June, 1992: Lightning Precursor Signatures from Dual-Polarization Radar Measurements of Storms. Presented at: *URSI Commission F Open Symposium,* Ravenscar, UK.

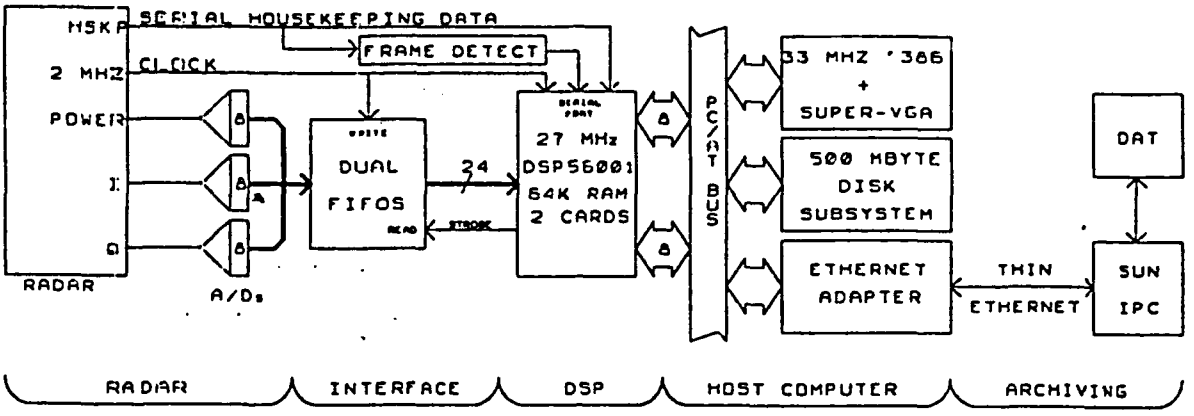

Figure 1. Data acquisition/display system block diagram.

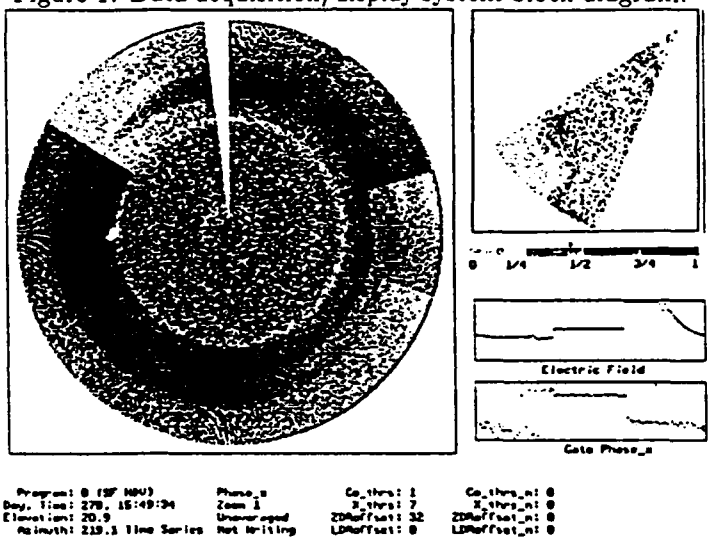

Figure 2. Default display format.
Polar Time vs. Range (ρ_x) plus PPI (ϕ_x)

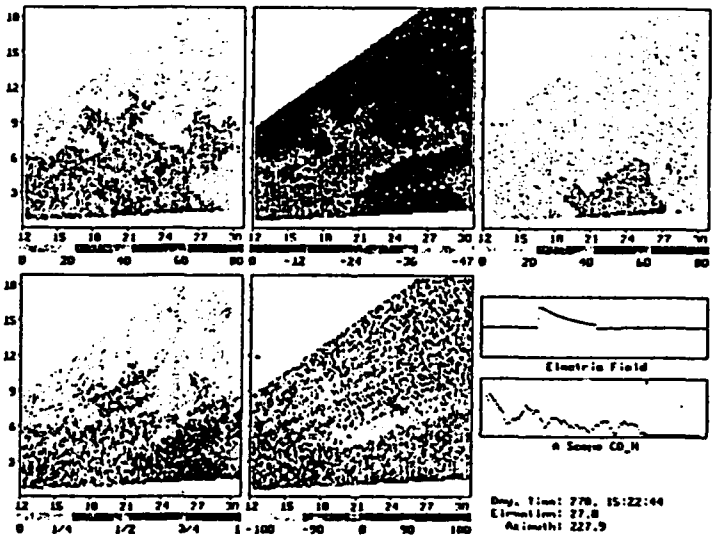

Figure 3. Alternate display format.
Z_{hh}, LDR, Z_{hv}, ρ_x, and ϕ_x: RHI scan.

A PC-BASED REAL-TIME RADAR SIGNAL PROCESSING AND DISPLAY SYSTEM

Grant Gray William Rison Paul R. Krehbiel
Tiehan Chen
Geophysical Research Center
New Mexico Institute of Mining and Technology,
Socorro, New Mexico 87801

June 15, 1993

1. Introduction

Inexpensive personal computers and workstations are now fast enough to handle the real-time task of displaying and archiving meteorological radar data. Digital Signal Processing (DSP) chips have greatly simplified the computational tasks involved in extracting parameters from a radar return. Last year we reported on a design for a small and inexpensive signal processing and display system for the New Mexico Tech Wideband, Coherent Radar (Rison, 1991). We implemented the design and have operated and improved it now for over a year.

For the New Mexico Tech multiparameter radar we need to compute and display several parameters, including reflectivity (Z_{hh}), mean Doppler velocity ($\overline{v}$), differential reflectivity (Z_{dr}), linear depolarization ratio (LDR), and complex cross-polar correlation amplitude (ρ_x) and phase (ϕ_x). Currently available digital signal processing (DSP) chips provide the computational power to process meteorological radar signals in real time. DSP chips are designed to perform very fast floating point or integer multiplies and adds, since these operations make up the bulk of signal processing algorithms. DSP chips are generally well supported by the manufacturers with extensive software tools such as assemblers, simulators, compilers and debuggers. Inexpensive plug-in boards with one or more DSP chips, I/O interfaces, and memory are commercially available.

A block diagram for the processing/display system is shown in Figure 1. It consists of four major sections — the radar data stream, the hardware interface between the radar and the DSPs, the DSPs themselves, and the host computer with its display monitor. The system also incorporates an instrumentation recorder with a digital interface for recording raw time series data from the analog to digital converters.

2. Radar

The radar is a multi-parameter radar which can transmit both horizontally and vertically polarized pulses, or right- and left-hand circularly polarized pulses, and simultaneously receive both co- and cross-polar returns through two independent receiver chains. It can transmit either single frequency for Doppler measurements, or broadband noise for fast-scanning reflectivity measurements. The received return is digitized at a 1 MHz rate, giving a range resolution of 150m. For each range gate, the radar produces 6 bytes of data — signal power, and I and Q for both vertical and horizontal polarizations. Signal power can be either logarithmic or linear, depending on the operating mode of the receiver. The 6 bytes of data for each range gate are formated as two 24 bit words — the three bytes of the horizontal return, followed by the three bytes of the vertical return — which are clocked out at a 2 MHz rate.

The sequence of transmitted pulses is flexible. A typical transmission sequence for Doppler studies is to transmit single-frequency pulses at a 4 kHz PRF, with alternating transmitted po-

larization from pulse to pulse. The radar is capable of many other modes including single polarization horizontal or vertical, noise transmissions interlaced with coherent transmissions, and passive radiometric mode. The DSP cards decode the current mode of the radar transmitter/receiver from the housekeeping data stream and activate the proper code section to handle that mode.

The azimuth, elevation, transmitted polarization, attenuation settings, time, and other auxiliary data are clocked out serially with the digitized return data. A 24 bit sync word is embedded in the serial data stream to indicate the start of each pulse. At 4 kHz PRF (making 250 range gates), each pulse results in 500 twenty-four bit data words and 500 bits of serial data, clocked out at 2 MHz. If so desired, this stream of time-series data may be recorded on the instrumentation recorder. The serial bit stream is also recorded on a single track of the instrumentation recorder. The interface is so designed so that the instrumentation recorder output is indistiguishable from live radar data from the point of view of the DSP's.

3. Interface

A minimal hardware interface buffers the data to the DSP. The parallel data is clocked into alternating First-In-First-Out (FIFO) buffers, so the DSP can access data asynchronously. While one FIFO bank is being written to by the radar, the other bank is being read asynchronously by the DSPs. The banks are switched at each radar pulse. The serial housekeeping stream goes directly into the DSP. A sync detector circuit monitors the serial data, searching for the sync word. When the sync detector recognizes the sync word, it asserts a frame detect output, which the DSP uses to break the serial data stream into individual data words. While the FIFOs are being filled with data from the current pulse, the DSP decodes the serial data to determine how it should process the buffered data.

4. DSP

The computational heart of the system is the 27 MHz Motorola 56001 DSP chip executing 13.5 Million Instructions Per Second (MIPS). Each instruction cycle of the 56001 can incorporate up to five functions — an arithmetic operation on data (such as a multiply/accumulate), two parallel data moves, and two address calculations. The 56001 offers a 24 bit word width, a 24 bit parallel interface for data I/O, built-in hardware for serial I/O, and an 8 bit host port to communicate with a host computer. A powerful data handling feature of the 56001 is its zero-overhead interrupt mode. After receiving an interrupt, the 56001 can execute two instructions (such as moving data from memory to the host port) without having to save registers and branch to an interrupt service routine.

We purchased two commercial DSP56001 boards each with 64 k words of zero wait-state static RAM memory. These boards plug into the bus of the host computer (a 20 MHz 386 PC/AT clone, in this case). All software development is performed on the host, and the assembled programs are uploaded through the host port to the DSP cards. At present one DSP card computes incoherent quantities such as P_{hh} (signal power), LDR, and Z_{dr}, and the other card handles coherent parameters, such as $\overline{v}$, or ρ_x and ϕ_x.

The Motorola 56001 DSP has built-in hardware to format the serial data stream into 16 bit words. Once formatted, the DSP can determine the polarization and type (noise or single frequency) of the transmitted pulse, from which the DSP determines how to handle the parallel data buffered in the FIFOs. For example, to compute differential reflectivity, the DSP first waits until the FIFOs are filled with data from a horizontally-polarized pulse. It then reads the data from the FIFOs, discarding all data except $\log P_{hh}$, the horizontally-polarized power, which it stores. For the next (vertically polarized) pulse, it reads the parallel data, discarding all but $\log P_{vv}$, the vertically-polarized power. It then calculates $\log P_{hh} - \log P_{vv}$, and accumulates the difference in an array. After averaging for a selectable number of pulses the DSP's are ready to send processed data to the host computer. The 8 bit data words are mapped into one of 256 colors to be displayed on the monitor. The non-coherent DSP can compute P_{hh}, Z_{DR}, and L_{DR} simultaneously. Thus, for each set of pulses, 750 bytes of information are calculated in this DSP. In a similar fashion, the other DSP discards power and uses the I and Q values

to compute $\overline{v}$ or ρ_x and ϕ_x for an additional 250 or 500 bytes of information per ray.

The host computer needs to determine from the azimuth and elevation data where to map a range gate on the display monitor. To ease the computational demands on the host computer, the DSP converts the azimuth and elevation into a single number which the host computer can use as an offset into a look-up table to determine the appropriate mapping. After the pulses are accumulated, the DSP signals the host computer that data are available, and initiates the transfer through the DSP's host port. The DSP side of the transfer is done through zero-overhead interrupts, so the DSP can be processing the next set of pulses while the transfer of the last set takes place.

5. Host Computer

The host computer uploads code to the DSP's, controls operation of the DSP's, generates the display, and controls data archival. After the DSP's have processed a set of samples, they signal the host that data are available. The host then reads and displays the data, and sends the data to disk, if recording is enabled. The first data item read is the offset into the look-up table which the DSP computed from the azimuth and elevation. This is followed by 250 bytes of data for each of the radar data products.

In displaying a ray of radar data, a range gate may be mapped into more than one pixel. The host computer uses the offset it reads from the DSP to look into a table which specifies into how many pixels the range gate maps. It then uses the same offset as an index into another table, from which it reads a pointer that points to a memory location holding the address of the first pixel to map. It maps the appropriate color for the range gate into that pixel, increments the pointer to get the address of the next pixel to map, and continues for all the pixels required for that particular range gate. It then increments the table offset, and repeats the process for the next range gate. Thus, the host computer does not need to do any calculations itself; it determines display locations by means of very quick look-ups in pre-computed tables. This requires a large amount of RAM in which to store the tables — the 4 Mbytes in our computer is sufficient.

Though we acquired a 20 MHz 386 PC/AT clone for the original system, other computers would work as well. DSP cards are available for VME bus, NU bus, and S bus, and excellent graphics capability can be obtained for most computers based on these buses. We chose a PC/AT clone because of price, speed, the availability of software tools for programming and debugging the DSP, and the ease of interacting with the hardware under the DOS operating system. We currently write data directly to a 500 Mbyte disk internal to the PC. After operations have terminated for the day we then transfer the data over Ethernet to a Sun IPC and then to a Digital Audio Tape (DAT) for permanent archival. In the next evolutionary step of the system, we will include a SCSI interface on the PC for direct archival to DAT or Exabyte tapes. Data will also be broadcast over Ethernet for use by remote workstations or PCs.

We are currently using Watcom's Optimizing C Compiler for the PC data acquisition and display code. This compiler produces protected mode code, giving the software direct access to all the 386 memory. The resulting code runs 2-3 times as fast as similar algorithms running in real mode. For the DSP code we are using the standard Motorola assembler/linker.

6. Display

The Super-VGA display offers 800 horizontal by 600 vertical pixels with 256 colors available for each pixel. We considered 16 colors per quantity to be adequate for an operational display, but we use a few others for special functions. The default primary display is shown in Figure 2. The 500 x 500 pixel area in the upper left defaults to a PPI presentation. The smaller 250 x 250 pixel area in the upper right defaults to RHI, but the roles of two areas may be reversed. The large area is also used for time vs. range displays for observations at fixed antenna angles. Both rectagular and polar time vs. range displays are available. The polar version depicts time as advancing azimuth angle, while the rectangular format has time as the horizontal axis. Format switching amongst RHI, PPI, and time vs. range may be commanded to automatically follow antenna motion, if desired. The following

parameters may be displayed: Phh, Pvv, Zhh, Zvv, Phv, Z_{dr}, LDR, $\overline{v}$, ρ_x, or ϕ_x. The images may be zoomed up to 4:1 and the effective center of the screen may be offset in any direction. On the 20 MHz 386 the angular ray painting rate is 25 degrees/sec. On a 50 MHz 486 the rate was over 60 degrees/second. Two additional rectangular plotting areas are positioned below the small RHI area on the right side of the screen. The upper rectangle is pemanently assigned to display a "strip-chart" representation of local electric field. The lower rectangle presents either a value vs. range display of the parameter presently displayed on the PPI/RHI, or a strip-chart of the value of the parameter in one selected gate. Selected alphanumeric quantities, including time, angles, scaling parameters, etc., are displayed in the lower portion of the screen. Data acquisition controls consist of toggling recording on and off, and selecting a filename for the archive file. Nearly all commands to the display and data acquisition functions consist of individual keystrokes on the host computer keyboard.

The alternate display, shown in Figure 3, contains five 250 x 250 rectangular areas and simultaneously presents Z_{hh}, Z_{dr}, LDR, and either ρ_x and ϕ_x , or $\overline{v}$. The alternate display also contains the strip-chart displays of electric field and parameter values described above as well as a portion of the alphanumerics from the primary display.

7. Conclusion

Excluding labor, the entire signal processing and display system cost less than $10,000 — about $4,000 for the host computer and monitor, $2,000 for the two DSP cards, $1,000 for the software, and $1,500 for parts to build the hardware interface. The 20 MHz 386 PC/AT was marginally fast enough to handle both archival and display generation, and we plan to replace it with a faster 50 MHz 486. We will then include the user interface for antenna control in the host, particularly if we identify a multitasking operating system suitable for real-time work on PC's.

The use of somewhat higher priced floating point DSP chips such as Motorola's 96002 or TI's TMS320C30 or -C40 would eliminate some of the scaling and arithmetic overflow problems encountered using the 56001. The fast direct memory access capability of some of the DSP chips recently released could eliminate the need for the FIFO memories altogether, thus offseting some of the higher DSP costs.

We have experimented with integrating data sets from other instruments with this radar display. One such data source was the New Mexico Tech Lightning Interferometer (Rhodes, 1992). A sample of the lightning display integrated with a smaller-scale version of the radar display is shown in Figure 4. In the real-time version the lightning leader location information would be processed on another DSP card inside the host, or in another host linked to the display computer via Ethernet.

With recent sharp drops in the price of workstations, such as the Sun IPC and IPX, it is enticing to consider using one of these systems as a host in order to have the power of Unix in a multitasking, multiuser environment, plus the networking advantages inherent in these systems.

REFERENCES:

Barron, R., G. Gray, J. Lutz, 1986: New Features for NCAR Radars. Preprints: *22nd Conf. on Radar Meteorology.* Amer. Met. Soc. Snowmass. V2. pp 124-125.

Gray, G., et al, 1975: Real-time Color Display for Meteorological Radar. Preprints: *16th Conf. on Radar Meteorology.* Amer. Met. Soc. Houston.

Gray, G., et al, 1989: A New Programmable Signal Processor for NCAR Meteorological Radars. Preprints: *24rd Conf. on Radar Meteorology.* Amer. Met. Soc. Tallahassee.

Rhodes, C. T., X. Shao, R. Thomas, P. Krehbiel, C. Hayenga, 1992: Observations of Lightning Phenomena Using Radio Interferometry. Submitted to: *Journal of Geophysical Research.*

Rison, W., et al, 1991: Design of a PC-based Real-time Radar Display. Preprints: *25th International Conference on Radar Meteorology.* Amer. Met. Soc. Paris.

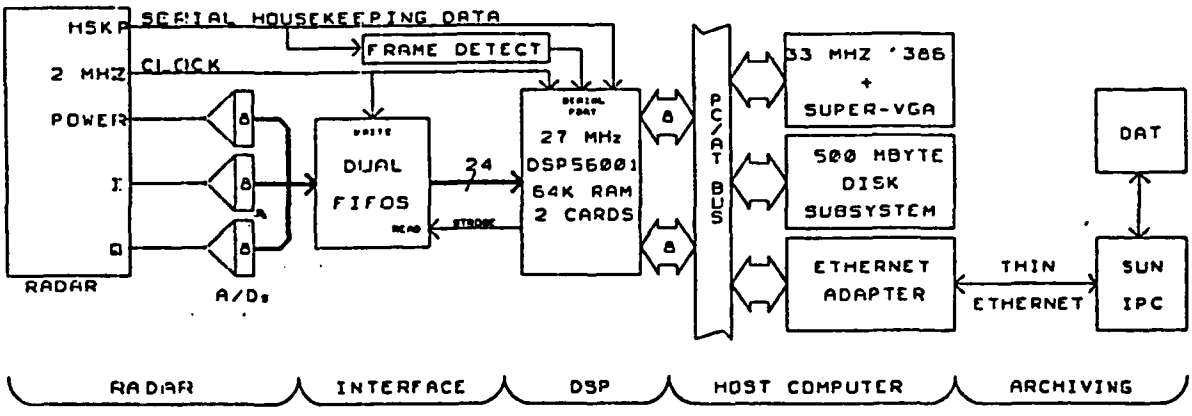

Figure 1. Data acquisition/display system block diagram.

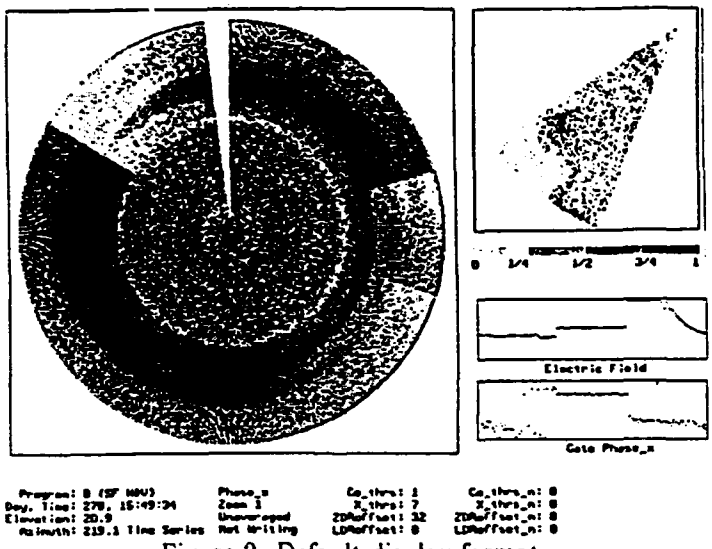

Figure 2. Default display format.
Polar Time vs. Range (ρ_x) plus PPI (ϕ_x)

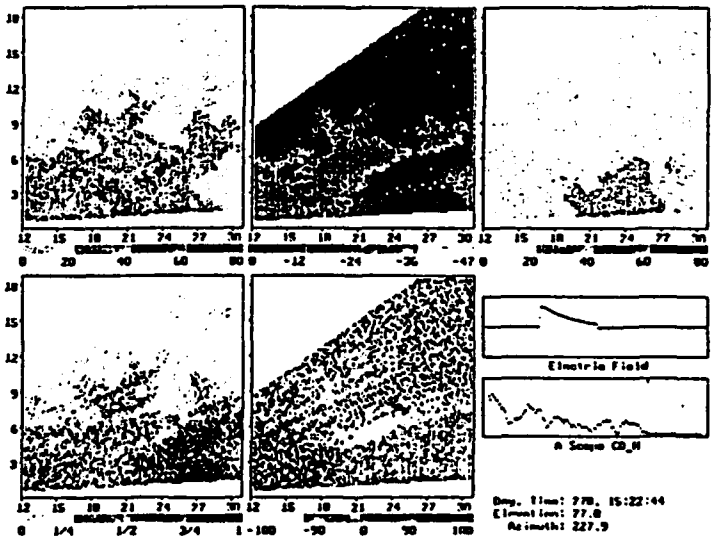

Figure 3. Alternate display format.
Z_{hh}, LDR, Z_{hv}, ρ_x, and ϕ_x: RHI scan.

Ninth International Conference on Atmospheric Electricity, St. Petersburg, Russia, June, 1992.

Dual-Polarization Radar Signatures of the Potential for Lightning in Electrified Storms

Paul Krehbiel, Tiehan Chen, Stephen McCrary, William Rison, Grant Gray, Thomas Blackman, Marx Brook

Langmuir Laboratory, Geophysical Research Center
New Mexico Tech, Socorro, NM 87801

Abstract. *Real-time correlation and display of the co-polar and cross-polar radar returns from electrically active storms has provided dramatic indications of the buildup of electric stress in the storms, and of its collapse at the time of lightning. Following up on the pioneering work of Hendry and McCormick, strong correlations are observed above the 0 ° C level in the middle and upper parts of storms that are indicative of the presence of electrically aligned particles. Regions of strong correlation are readily identified in scanning a storm, and provide an excellent indicator of the potential for lightning in the storm. The correlation values have been used to predict the occurrence of individual lightning discharges in storms; in addition, they have been used to detect the onset of electrification and to tell when a storm is finished producing lightning.*

1. Introduction. In a pioneering study, Hendry and McCormick (1976) of the National Research Council in Canada reported radar observations which indicated that particles were being electrically aligned in the upper levels of thunderstorms. The observations were made using a dual-channel circular polarization radar which operated at 16.5 GHz, and were obtained by coherently correlating the co-polar (e.g. RHC) and cross-polar (LHC) returns from a storm. Large correlation coefficients, indicative of a high degree of common particle orientation, were observed in the upper parts of storms. The correlation values decreased at the time of lightning discharges and regenerated between discharges. Lightning was sometimes also observed to *increase* the correlation or alignment.

In this paper we describe dual-polarization observations which confirm and extend Hendry and McCormick's results. The observations were made at Kennedy Space Center, Florida, as part of the Convective and Precipitation/Electrification (CaPE) program conducted there during the summer of 1991.

2. Measurements. For the measurements of this study, the radar transmitted alternate pulses of right- and left-hand circular polarization, and simultaneously received the co-polar and cross-polar returns from each pulse. The receiver outputs were digitized, processed and displayed in real time. The processing was accomplished with PC-based digital signal processors and the results were displayed on a high resolution monitor of the host PC. The radar operated at 9.8 GHz (3 cm wavelength) with 20 kW peak transmitted power and utilized a circularly-symmetric Cassegrain antenna with a corregated feed to maximize polarization purity.

For detecting the presence of aligned particles, the simultaneous co- and cross-polar returns for a given transmitted polarization were coherently correlated to give the squared magnitude $|\rho|^2$ and phase ϕ of the correlation function. The various quantities were displayed in PPI and RHI format to show their structure as the radar scanned through a storm. Lightning occurrences were detected using an electric field change meter and a directional optical detector attached to the radar antenna.

3. Results. Figures 1a and 1b show vertical cross-sections of the various polarization variables in a storm on Day 278, 1991. (The scans do not extend down to ground level because radar transmissions at KSC were restricted at low elevation angles.) The two sets of cross-sections are from sequential scans just before and after an intracloud lightning discharge occurred in the storm, and were separated by less than 20 seconds in time. The figures show the co-polar and cross-polar reflectivity structure, the resulting circular depolarization ratio (CDR), and the squared magnitude and phase of the co-polar – cross-polar correlation. The storm was 15 to 27 km distant from the radar and extended up to 13 km altitude (MSL), with two cells being evident in the co-polar reflectivity.

In the scan just prior to the lightning (Figure 1a), two regions of strong correlation ($|\rho|^2 > 0.75$) ex-

Figure 1a. Vertical cross-sections of *a*) co-polar reflectivity, *b*) circular depolarization ratio, *c*) cross-polar reflectivity, and the correlation quantities $|\rho|^2$ (*d*) and ϕ (*e*), just prior to a lightning discharge in the storm. The distance scale is 3 km per tic mark. Contours are at 20 dB intervals for reflectivity, 12 dB for CDR, 0.25/1.0 for $|\rho|^2$ and $\pi/2$ for ϕ.

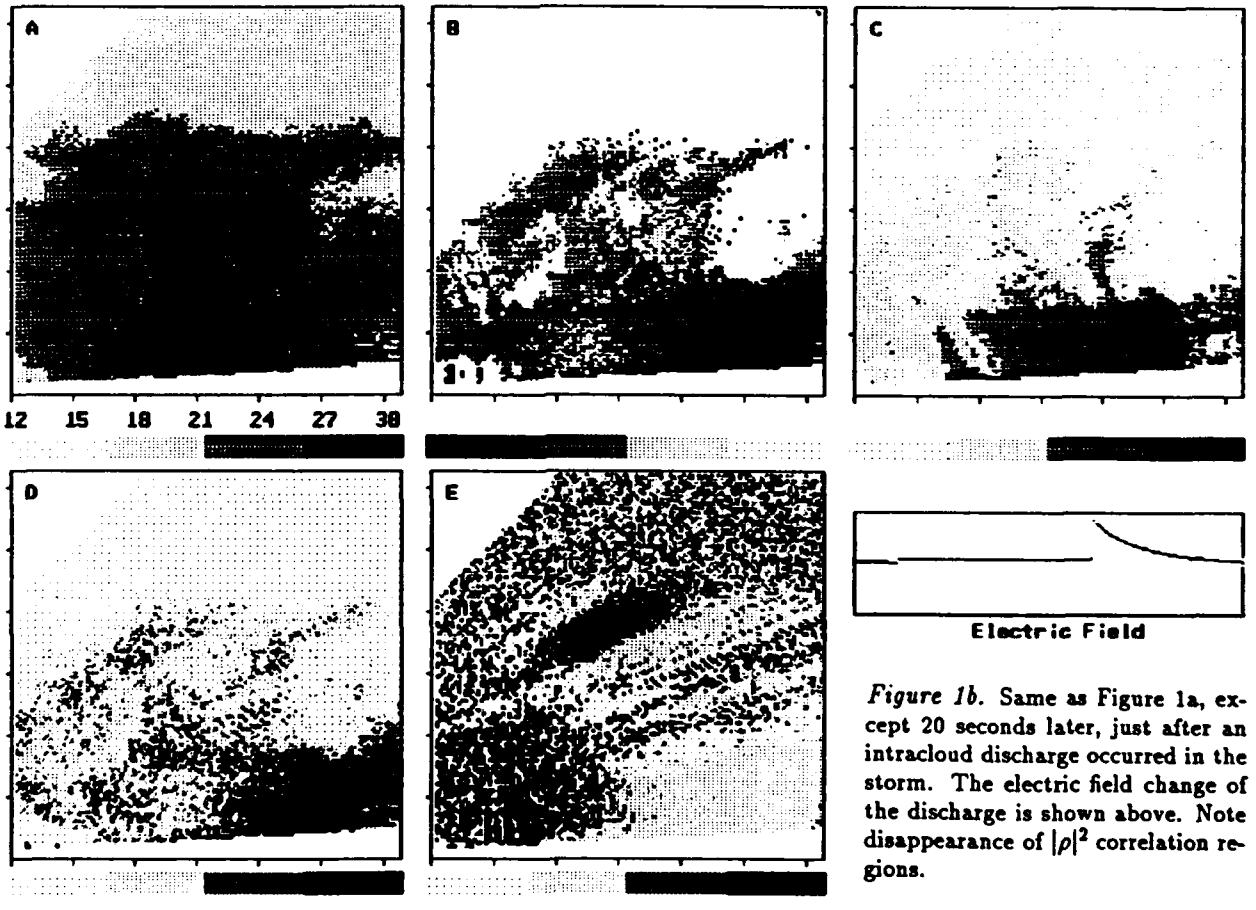

Figure 1b. Same as Figure 1a, except 20 seconds later, just after an intracloud discharge occurred in the storm. The electric field change of the discharge is shown above. Note disappearance of $|\rho|^2$ correlation regions.

isted at mid-levels (6-9 km MSL) in the far cell and in the upper part (9-12 km) of the near cell. These were associated with local maxima in the cross-polar reflectivity and CDR. After the discharge, the correlation regions had essentially disappeared and the associated cross-polar returns and CDR had diminished in intensity. The co-polar returns were unchanged in the two scans, as were the cross-polar returns and CDR values below the melting level, at about 4–4.5 km altitude.

Correlation regions such as described above were observed to regenerate gradually until the next discharge, which would wipe them out and restart the cycle. Figures 2a and 2b show how the polarization quantities varied with time at a fixed location in the electrically active region of two storms. Each figure shows 5 minutes of data and includes the electric field change record of lightning occurrences. The data of Figure 2a are from 8.7 km altitude in a storm where lightning occurred at nearly regular time intervals; each discharge was accompanied by sudden decreases in both the cross-polar power and the correlation magnitude, as well as by rapid phase excursions. Figure 2b shows more complex behavior at 10.4 km altitude in another storm system in which the lightning activity was irregular and superimposed on activity from other storms. In one instance near the beginning of the Figure 2b data, the correlation increased at the time of lightning.

4. Discussion. Regions of strong co-polar – cross-polar correlation are readily identified in scanning through a storm and appear always to be present in electrified storms. As noted by Hendry and McCormick (1976), the fact that the correlation values are affected by lightning and are observed above the 0 °C level indicates that they are caused by the electrical alignment of ice particles, presumably crystals. The effect of alignment upon the correlation is suprisingly strong, and produces 'signatures' as in Figure 1a which are found to be an excellent indicator of the potential for lightning in a storm. We have been able to predict the occurrence of numerous discharges from the real-time correlation observations.

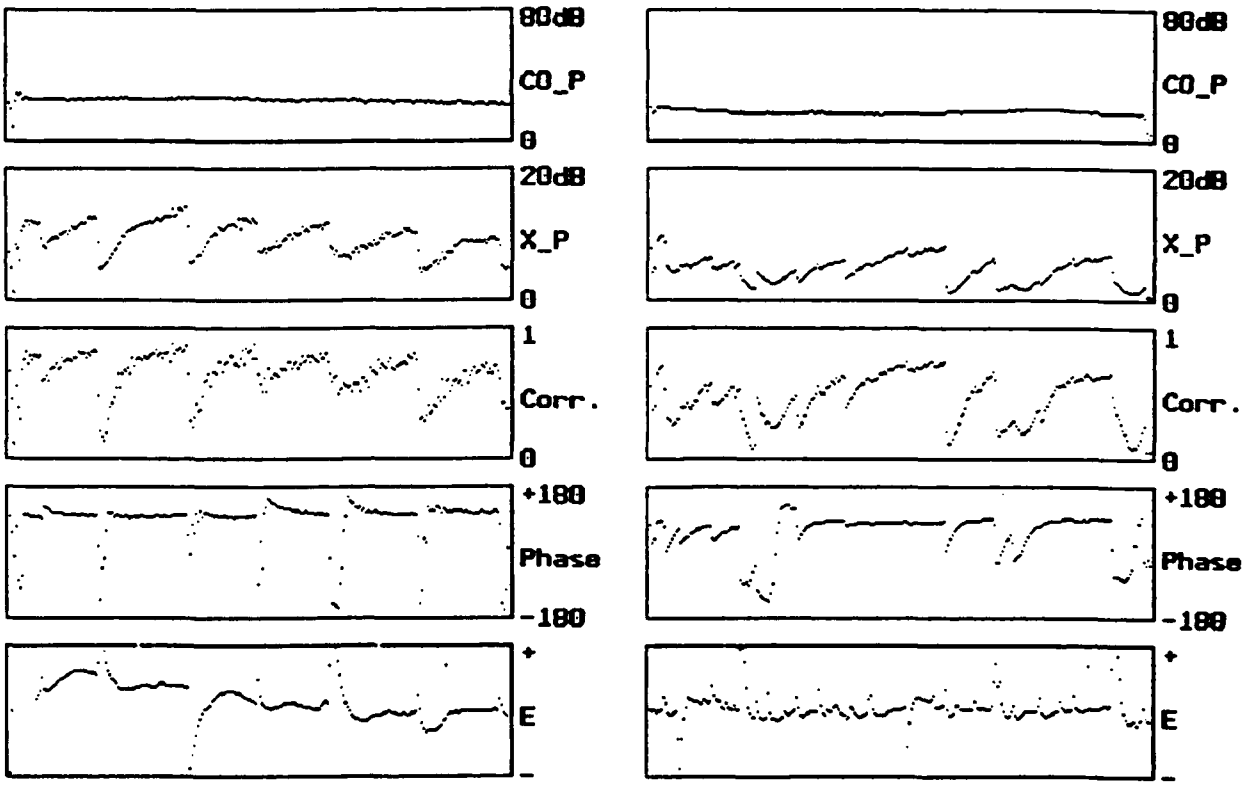

Figure 2. Examples of the time variation of the polarization variables over 5-minute time intervals at a fixed location in two lightning-producing storms. Shown from top to bottom are the co-polar and cross-polar reflectivities, the squared magnitude and phase of the correlation function, and the lightning electric field change. The data are from altitudes of 8.7 km (Figure 2a, left) and 10.4 km (Figure 2b, right).

The correlation measurements have also been used to detect the onset of electrification in several storms, before the first lightning discharge. During the initial stages of storms, and often in later stages as well, the region of strong correlation is observed between about 6 and 8 or 9 km altitude MSL and is co-located with the storm core. This coincides approximately with the altitude of the main negative charge in storms. In one storm, the altitude of the correlation region was observed to decrease as the storm dissipated, down to just above the melting level. In several instances, storms which were decaying and had not produced lightning for several minutes were observed still to have large correlation values within them, and subsequently went on to produce additional discharges. Storms which are not electrified exhibit weak correlations above the 0 °C level.

Although aligned particles themselves will produce cross-polar returns that are correlated with the co-polar returns, a more important effect is that the circularly polarized radiation is progressively depolarized as it propagates through the aligned particle region (Hendry and McCormick, 1976). As the signal is depolarized, returns of a cross-polar sense are produced even from non-depolarizing particles, that are perfectly correlated with the co-polar return.

Depolarization is a major effect in liquid precipitation due to aerodynamic flattening of drops, and provides a means of remotely sensing the rainfall (e.g. Bringi et al., 1991). The depolarizing effect of rain is seen below 4 km in Figure 1, where CDR and $|\rho|^2$ are seen to increase gradually through regions of stronger precipitation and to maintain large values on the far side of the precipitation. The electrical correlation regions exhibit similar features, indicating that they result primarily from propagation depolarization. This also explains the large magnitudes of the correlation. The alternate explanation is that a large fraction of the particles are aligned; while this could happen at the storm top, it would not occur in mixed precipitation regions, such as at mid-levels, where strong correlations are also observed.

The correlation phase ϕ provides a measure of the direction of particle orientation. The phase values shown in Figure 1a indicate that the particles in the upper part of the storm were oriented in an approximately vertical direction. Liquid precipitation is known to be horizontally oriented, and the phase values in the lower part of the storm are correspondingly different. Intermediate phase values are observed at other locations in the storm.

Alignment correlations are observed with linearly polarized transmissions (horizontal and vertical) but are much less pronounced than with circular polarization. This is because minimal or no depolarization occurs when the particles are aligned parallel or perpendicular to the linear radar polarization.

As seen in Figure 2, alignment effects can also be detected from incoherent measurements of the cross-polar power and CDR. This was noted by Hendry and McCormick (1976) and was previously detected with the radar of this study, using linear polarizations (Krehbiel et al., 1991). As can be seen from Figure 1a, aligned particles produce regions of locally enhanced cross-polar returns and depolarization ratios above the 0 °C level. While incoherent observations by themselves could provide indications of electrical alignment, the indications are not as strong and dramatic (or certain) as those of the correlation results.

5. Acknowledgments. This research was supported by the U.S. Air Force Office of Scientific Research under Grant AFOSR-89-0450.

6. References.

Bringi, V.N., V. Chandrasekar, P. Meischner, J. Hubbert, and Y. Golestani (1991): Polarimetric radar signatures of precipitation at S- and C-bands. *Proc. IEE-F*, **138**, 109–119.

Hendry, A., and G.C. McCormick (1976) Radar observations of the alignment of precipitation particles by electrostatic fields in thunderstorms. *J. Geophys. Res.*, **81**, 5353–5357.

Krehbiel, P.R., W. Rison, S. McCrary, T. Blackman, and M. Brook (1991): Dual-polarization radar observations of lightning echoes and precipitation alignment at 3 cm wavelength. Preprints, 25th Conf. Radar Meteorol., Paris, Amer. Meteor. Soc., 901–904.

URSI Commission F Open Symposium,
Ravenscar, UK, June 1992.

Lightning Precursor Signatures from Dual-Polarization Radar Measurements of Storms

Paul Krehbiel, Tiehan Chen, Stephen McCrary, William Rison, Grant Gray, Thomas Blackman, Marx Brook

Langmuir Laboratory, Geophysical Research Center
New Mexico Tech, Socorro, NM 87801

Abstract. *Real-time correlation and display of the co-polar and cross-polar radar returns from electrically active storms has provided dramatic indications of the buildup of electric stress in the storms, and of its collapse at the time of lightning. Following up on the pioneering work of Hendry and McCormick, strong correlations are observed above the 0 °C level in the middle and upper parts of storms that are indicative of the presence of electrically aligned particles. Regions of strong correlation are readily identified in scanning a storm, and provide an excellent indicator of the potential for lightning in the storm. The correlation values have been used to predict the occurrence of individual lightning discharges in storms; in addition, they have been used to detect the onset of electrification in storms and to tell when a storm is finished producing lightning.*

1. Introduction. In a pioneering study, Hendry and McCormick (1976) of the National Research Council in Canada reported radar observations which indicated that particles were being electrically aligned in the upper levels of thunderstorms. The observations were made using a dual-channel circular polarization radar which operated at 16.5 GHz, and were obtained by coherently correlating the co-polar (e.g. RHC) and cross-polar (LHC) returns from a storm. Large correlation coefficients, indicative of a high degree of common particle orientation, were observed in the upper parts of storms. The correlation values decreased at the time of lightning discharges and regenerated between discharges. Lightning was sometimes also observed to *increase* the correlation.

In this paper we describe dual-polarization observations which confirm and extend Hendry and McCormick's results. Real-time processing and display of the co-polar – cross-polar correlation has shown that regions of strong correlation are detected in the middle and upper levels of storms. The correlation 'signatures' have been found to provide an excellent indicator of the potential for lightning in a storm. The observations were made at Kennedy Space Center, Florida, as part of the Convective and Precipitation/Electrification (CaPE) program conducted there during the summer of 1991.

2. Measurements. The radar used in this study was a polarization-diverse system in which the polarization of the transmitted signal was alternated from pulse to pulse, between either right- and left-circular polarization or (with a different orthomode transducer) between horizontal and vertical linear polarizations. The co-polar and cross-polar returns were simultaneously received, both coherently and incoherently, and the receiver outputs were digitized, processed and displayed in real time. The processing was accomplished with PC-based digital signal processors and the results were displayed on a high resolution monitor of the host PC. In addition, a high-density digital recorder was used to record complete time series data. The radar is a pulsed system that operates at 9.8 GHz (3 cm wavelength) with 20 kW peak transmitted power. The radar has a circularly-symmetric Cassegrain antenna with a corregated feed to maximize polarization purity.

For detecting the presence of aligned particles, the simultaneous co- and cross-polar returns for a given transmitted polarization were coherently correlated to give the squared magnitude $|\rho|^2$ and phase ϕ of the correlation function. The various quantities were displayed in PPI and RHI format to show their structure as the radar scanned through a storm. All results presented in this paper are from circularly polarized transmissions, which were found to be more sensitive to alignment effects than linear polarization. Lightning occurrences were detected using an electric field change meter and a directional optical detector attached to the radar antenna.

3. Results. Figures 1a and 1b show vertical cross-sections of the various polarization variables in a storm on Day 278, 1991. (The scans do not extend down to ground level because radar trans-

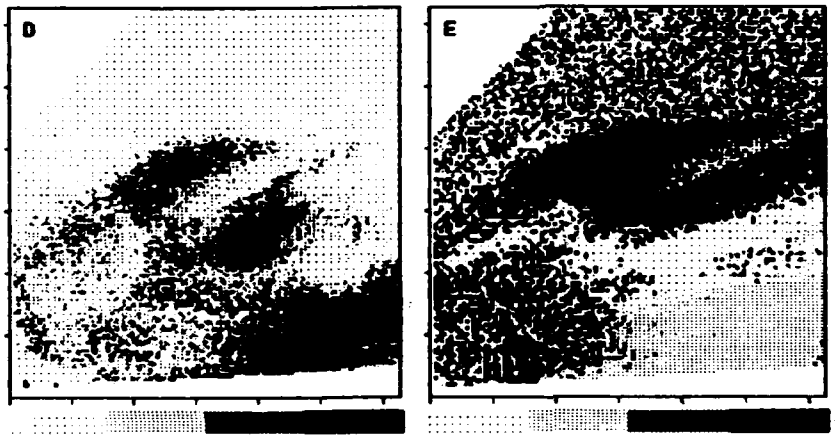

Figure 1a. Vertical cross-sections of *a*) co-polar reflectivity, *b*) circular depolarization ratio, *c*) cross-polar reflectivity, and the correlation quantities $|\rho|^2$ (*d*) and ϕ (*e*), just prior to a lightning discharge in the storm. The distance scale is 3 km per tic mark. Contours are at 20 dB intervals for reflectivity, 12 dB for CDR, 0.25/1.0 for $|\rho|^2$ and $\pi/2$ for ϕ.

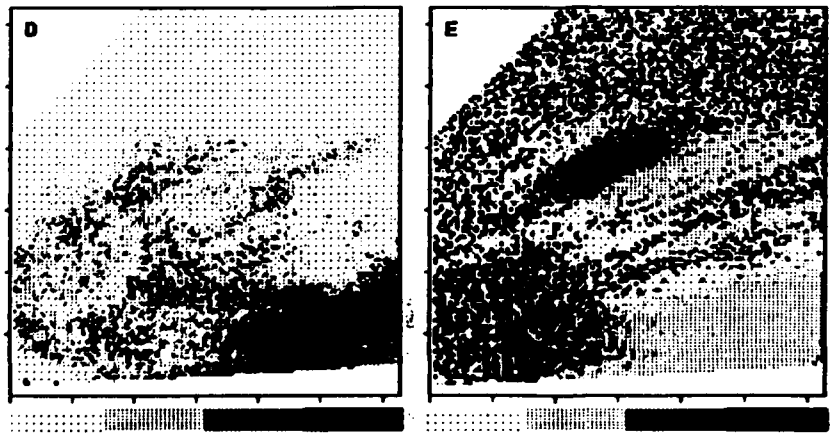

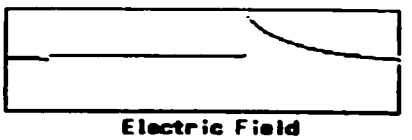

Figure 1b. Same as Figure 1a, except 20 seconds later, just after an intracloud discharge occurred in the storm. The electric field change of the discharge is shown above. Note disappearance of $|\rho|^2$ correlation regions.

missions at KSC were restricted at low elevation angles.) The two sets of cross-sections are from sequential scans just before and after an intracloud lightning discharge occurred in the storm, and were separated by less than 20 seconds in time. The figures show the co-polar and cross-polar reflectivity structure, the resulting circular depolarization ratio (CDR), and the squared magnitude and phase of the co-polar – cross-polar correlation. The storm was 15 to 27 km distant from the radar and extended up to 13 km altitude (MSL), with two cells being evident in the co-polar reflectivity.

In the scan just prior to the lightning (Figure 1a), two regions of strong correlation ($|\rho|^2 > 0.75$) existed at mid-levels (6-9 km MSL) in the far cell and in the upper part (9-12 km) of the near cell. These were associated with local maxima in the cross-polar reflectivity and CDR. After the discharge, the correlation regions had essentially disappeared and the associated cross-polar returns and CDR had diminished in intensity. The co-polar returns were unchanged in the two scans, as were the cross-polar returns and CDR values below the melting level, at about 4–4.5 km altitude.

Correlation regions such as described above were observed to regenerate gradually until the next discharge, which would wipe them out and restart the cycle. Figures 2a and 2b show how the polarization quantities varied with time at a fixed location in the electrically active region of two storms. Each figure shows 5 minutes of data and includes the electric field change record of lightning occurrences. The data of Figure 2a are from 8.7 km altitude in a storm where lightning occurred at nearly regular time intervals; each discharge was accompanied by sudden decreases in both the cross-polar power and the correlation magnitude, as well as by rapid phase excursions. Figure 2b shows more complex behavior at 10.4 km altitude in another storm system in which the lightning activity was irregular and superimposed on activity from other storms. In one instance near the beginning of the Figure 2b data, the correlation increased at the time of lightning.

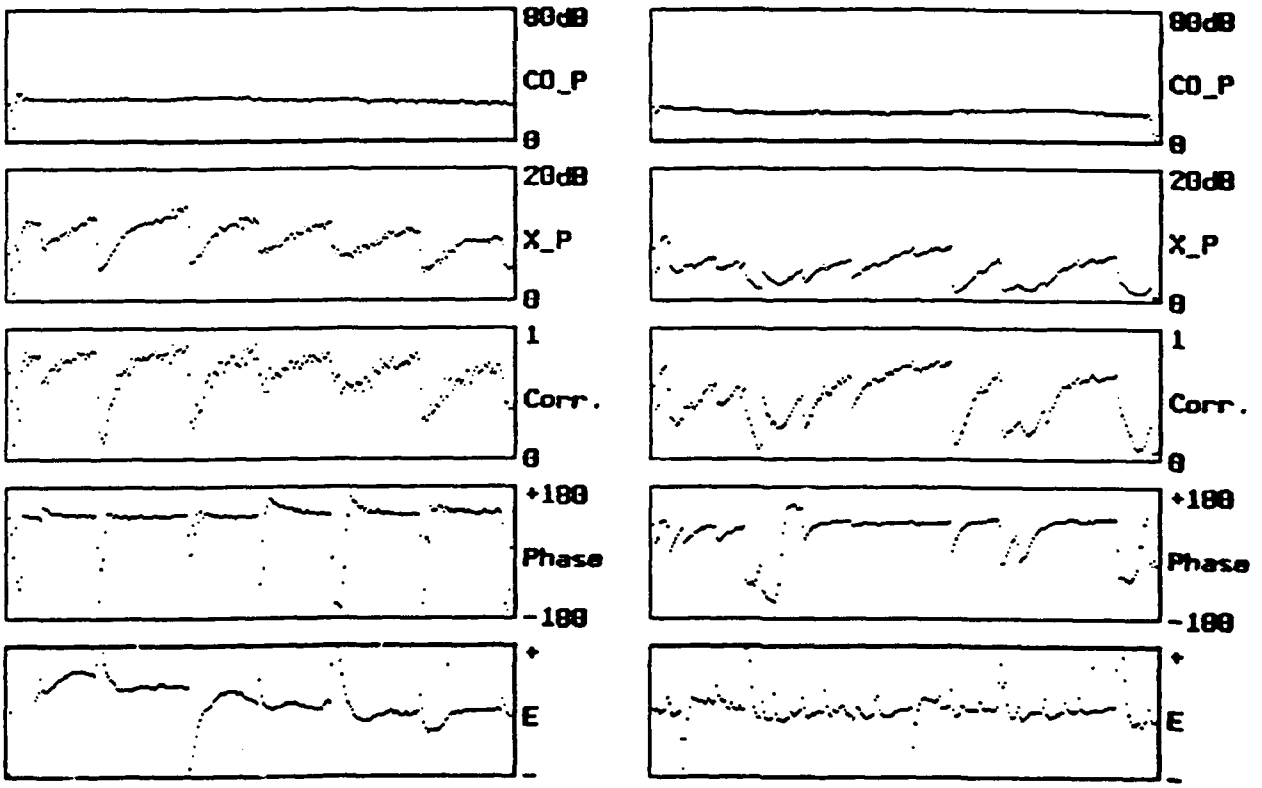

Figure 2. **Examples of the time variation of the polarization variables over 5-minute time intervals at a fixed location in two lightning-producing storms. Shown from top to bottom are the co-polar and cross-polar reflectivities, the squared magnitude and phase of the correlation function, and the lightning electric field change. The data are from altitudes of 8.7 km (Figure 2a, left) and 10.4 km (Figure 2b, right).**

In Figure 2a, each data point was the average of 12 sets of 32 transmitted pulses from a single range gate; this resulted in peak-to-peak fluctuations of about 0.1 (10 percent) in $|\rho|^2$. To illuminate the more complex behavior of Figure 2b, the signals were additionally averaged over 16 consecutive range gates (2.4 km distance) within the strong correlation region. In both cases, the $|\rho|^2$ record is seen to closely follow the logarithmic cross-polar power, indicating that the correlation value was affected primarily by the cross-polar signal-to-noise ratio, which tended to be small at the 30 km range of the observations. The correlation phase, which is indicative of particle orientation, was more accurately estimated, even at a single gate. Preliminary analysis of the phase values indicates that the particles of both figures were aligned in an approximately vertical direction.

4. Discussion. Regions of strong co-polar – cross-polar correlation are readily identified in scanning through a storm and appear always to be present in electrified storms. As noted by Hendry and McCormick (1976), the fact that the correlation values are affected by lightning and are observed above the 0 °C level indicates that they are caused by the electrical alignment of ice particles, presumably crystals. The effect of alignment upon the correlation is surprisingly strong, and produces 'signatures' as in Figure 1a which are found to be an excellent indicator of the potential for lightning in a storm. We have been able to predict the occurrence of numerous discharges from real-time correlation observations.

The correlation measurements have also been used to detect the onset of electrification in several storms, before the first lightning discharge. During the initial stages of storms, and often in later stages as well, the region of strong correlation is observed between about 6 and 8 or 9 km altitude MSL and is co-located with the storm core. In one storm, the altitude of the correlation region was observed to decrease as the storm dissipated, down to just above the melting level. In several instances, storms which were decaying and had not produced lightning for several minutes were observed still to have large correlation values within them, and subsequently went on to produce additional discharges. Storms which are not electrified exhibit weak correlations above the 0 °C level.

Aligned particles will produce correlated returns for two reasons (McCormick and Hendry, 1975): First, orthogonal returns from the particles themselves will be correlated. Second and more importantly, the radar signal will become progressively depolarized in propagating through a region of aligned particles, due to differential propagation effects (Hendry and McCormick, 1976). As the signal becomes depolarized, returns of a cross-polar sense are produced, even from non-depolarizing particles, that are perfectly correlated with the co-polar return. Differential propagation is a major effect in liquid precipitation due to aerodynamic flattening of drops, and is being studied by a number of investigators as a means of remotely sensing the rainfall (e.g. Holt, 1984; Sachidananda and Zrnic, 1986; Bringi *et al.*, 1991). The depolarizing effect of rain is seen below 4 km in Figure 1, where the depolarization ratio and correlation values are seen to increase gradually through regions of stronger precipitation and to maintain large values on the far side of the precipitation. The electrical correlation regions exhibit similar features and appear to result primarily from propagation depolarization. This would also explain the large correlation values that are observed. The alternate explanation would be that a large fraction of the particles are aligned; this was the initial inference by Hendry and McCormick (1976) and could happen at the storm top, but would not happen in mixed precipitation regions, such as at mid-levels, where strong correlations are also observed.

Alignment signatures are also observed with linearly polarized transmissions (horizontal and vertical) but are much less pronounced than with circular polarization. As is well understood, the depolarization effects of aligned particles will be independent of orientation for circular polarization, but will have nulls when symmetrical particles are aligned parallel or perpendicular to linearly-polarized transmissions.

As seen in Figure 2, alignment effects are readily detectable from incoherent measurements of the cross-polar power and CDR. This was noted by Hendry and McCormick (1976) and was previously detected with the radar of this study, using linear polarizations (Krehbiel *et al.*, 1991). As can be seen from Figure 1a, aligned particles produce regions of locally enhanced cross-polar returns and depo-

larization ratios above the 0 °C level in a storm. While incoherent observations by themselves could provide indications of electrical alignment, the indications are not as strong and dramatic (or certain) as those of the correlation results.

5. Acknowledgments. This research was supported by the U.S. Air Force Office of Scientific Research under Grant AFOSR–89–0450. Earlier development of the radar was supported by the U.S. Office of Naval Research and by the National Science Foundation.

6. References.

Bringi, V.N., V. Chandrasekar, P. Meischner, J. Hubbert, and Y. Golestani (1991): Polarimetric radar signatures of precipitation at S- and C-bands. *Proc. IEE*, **138**, 109–119.

Hendry, A., and G.C. McCormick (1976): Radar observations of the alignment of precipitation particles by electrostatic fields in thunderstorms. *J. Geophys. Res.*, **81**, 5353–5357.

Holt, A.R. (1984): Some factors affecting the remote sensing of rain by polarization diversity radar in the 3- to 35-GHz frequency range. *Radio Sci.*, **19**, 1399-1412.

Krehbiel, P.R., W. Rison, S. McCrary, T. Blackman, and M. Brook (1991): Dual-polarization radar observations of lightning echoes and precipitation alignment at 3 cm wavelength. Preprints, 25th Conf. Radar Meteorology, Paris, Amer. Meteor. Soc., 901–904.

McCormick, G.C., and A. Hendry (1975): Principles for the radar determination of the polarization properties of precipitation. *Radio Sci.*, **10**, 421–434.

Sachidananda, M., and D.S. Zrnic, (1986): Differential propagation phase shift and rainfall rate estimation. *Radio Sci.*, **21**, 235–247.

25th RADAR METEOROLOGY CONF.
PARIS, 1991

DESIGN OF A PC-BASED REAL-TIME RADAR DISPLAY

William Rison, Paul R. Krehbiel, Tiehan Chen, and Paresh Gondalia

Geophysical Research Center
New Mexico Institute of Mining and Technology,
Socorro, New Mexico 87801

Because of the computational power needed to process radar data in real time, radar displays are usually quite expensive. Display processors are often hardwired or micro-coded, making it difficult to adapt them to different modes of display. The New Mexico Tech Wideband, Coherent Radar is a multiparameter radar, for which we want to display mean Doppler velocity, mean reflectivity, differential reflectivity, and linear depolarization ratio. To do this, we built a display which is inexpensive, and is easy to reprogram for different display modes.

The current generation of digital signal processing (DSP) chips provides the computational power to process the radar data in real time. These chips are supported by the manufacturers with extensive software tools, such as assemblers, simulators, compilers and debuggers. Inexpensive plug-in boards with a DSP chip, I/O interfaces, and memory are commercially available. Workstations and personal computers are dropping in price and gaining in performance and display resolution, making them viable alternatives for use as dedicated displays.

The computational heart of our display is a 27 MHz Motorola 56001 DSP chip. This chip executes at 13.5 MIPS, and each instruction can carry out up to five functions—an arithmetic operation on data (such as a multiply-and-accumulate), two parallel data moves, and two address calculations. It operates on a 24-bit wide data word. It has a 24-bit parallel interface for data I/O, built-in hardware for serial I/O, and an 8-bit host port to communicate with a host computer. One nice feature of the 56001 is its zero-overhead interrupt mode. After receiving an interrupt, the 56001 can execute two instructions (such as moving data from memory to the host port) without having to save registers and branch to an interrupt service routine.

We purchased a commercial DSP board with a 56001 chip and 64 k words of zero-wait-state static RAM memory. This board plugs into the bus of a host computer (in our case, an IBM PC/AT 386 clone). All software development is performed on the host, and the assembled programs are uploaded through the host port to the 56001.

A block diagram for the display system is shown in Figure 1. It consists of four major parts—the radar data stream, the hardware interface between the radar and the DSP, the DSP itself, and the host computer with its display monitor.

• **Radar** The radar is a multi-parameter radar which can transmit both horizontally- and vertically-polarized pulses, and receives both polarizations. It can transmit either single frequency for Doppler measurements, or a broadband noise pulse for fast-scanning reflectivity measurements. The received return is digitized at a 1-MHz rate, giving a range resolution of 150 m. For each range gate, the radar produces 6 bytes of data—reflectivity, and I and Q for both vertical and horizontal polarizations. The 6 bytes of data for each range gate are formated as two 24-bit words—the three bytes of the horizontal return, followed by the three bytes of the vertical return—which are clocked out at a 2-MHz rate.

The sequence of transmitted pulses is selectable. A typical transmission sequence for Doppler studies is to transmit single-frequency pulses with a 4-kHz PRF, and to alternate transmitted polarization from pulse to pulse.

The azimuth, elevation, transmitted polarization, attenuation settings, time, and other auxiliary data are clocked out serially with the digitized return data. A 24-bit sync word is embedded in the serial data stream to indicate the start of each pulse. At 4 kHz PRF (making 250 range gates), each pulse results in 500 twenty-four bit data words and 500 bits of serial data, clocked out at 2 MHz.

• **Interface** A minimal hardware interface buffers the data to the DSP. The parallel data are clocked into First-In-First-Out (FIFO) buffers, so the DSP can access it asynchronously. The serial housekeeping stream goes directly into DSP. A sync detector circuit monitors the serial data, searching for the sync word. When the sync detector recognizes the sync word, it asserts a frame detect output, which the DSP uses to break the serial data stream into individual data words. While the FIFOs are being filled with data from the current pulse, the DSP decodes the serial data to determine how it should process the buffered data.

• **DSP** The Motorola 56001 DSP has built-in hardware to format the serial data stream into 16-bit words. Once formated, the DSP can determine the polarization and type (noise or single frequency) of the transmitted pulse, from which the DSP determines how to handle the parallel data buffered in the FIFOs. For example, to display differential reflectivity, the DSP executes the following algorithm. It waits until the FIFOs are filled with data from a horizontally-polarized pulse. It reads the data from the FIFOs, discarding all data except $\log Z_{hh}$, the horizontally-polarized reflectivity, which it stores. For the next (vertically polarized) pulse, it reads the parallel data, discarding all but $\log Z_{vv}$, the vertically-polarized reflectivity. It then calculates $\log Z_{hh} - \log Z_{vv}$, and accumulates the difference in an array. After accumulating for a set number of pulses (typically 64), the DSP averages the accumulated values, and is ready to send them to the host computer. The 8-bit data words map directly into one of 256 colors to be displayed on the monitor. The DSP can compute mean reflectivity, Z_{DR} and L_{DR} simultaneously. Thus, for each set of pulses, 750 bytes of information are calculated.

The host computer needs to determine from the azimuth and elevation data where to map the range gate on the display monitor. To ease the computational demands on the host computer, the DSP converts the azimuth and elevation into a single number which the host computer can use as an offset into a look-up table to determine the appropriate mapping. After the pulses are accumulated, the DSP signals the host computer that data are available, and initiates the transfer through the DSP's host port. The DSP side of the transfer is done through zero-overhead interrupts, so the DSP can process the next set of pulses while the transfer of the last set takes place.

• **Host Computer** The host computer acts as the system controller, and updates the display. The host uploads the code to the DSP to activate the appropriate display type. After the DSP has processed one set of pulses, and signals the host that data are available, the host reads and displays the data. The first item read is the offset into the look-up table which the DSP computed from the azimuth and elevation. This is followed by 250 bytes of data for each of the three display types.

For our display, we use a Super VGA (SVGA) graphics adapter and monitor, which has a resolution of 800x600 pixels of 256 colors. Because a range gate may be mapped into more than one pixel, the mapping is non-trivial. The host computer uses the offset it read from the DSP to look into a table which specifies into how many pixels the range gate maps. It then uses the same offset as an index into another table, from which it reads a pointer that points to a memory location holding the address of the first pixel to map. It maps the appropriate color for the range gate into that pixel, increments the pointer to get the address of the next pixel to map, and continues for all the pixels required for that particular range gate. It then increments the table offset, and repeats the process for the next range gate. Thus, the host computer does not need to do any calculations itself; it determines display locations by means of very quick look-ups in pre-computed tables. This requires a large amount of RAM to store the tables—the 4 MB in our computer is sufficient.

We use a PC/AT clone for our display, but other computers should work as well. DSP cards are available on VME bus, NU bus, and S bus cards, and computers which use these buses have very good graphics capabilities. We chose a PC/AT clone because of price, the availability of software tools for programming and debugging the DSP, and the ease of interacting with the hardware under the DOS operating system.

The entire display system cost less than $10,000—about $4,000 for the host computer and monitor, $1,000 for the DSP card, $1,000 for the software, and $1,000 for parts to build the hardware interface.

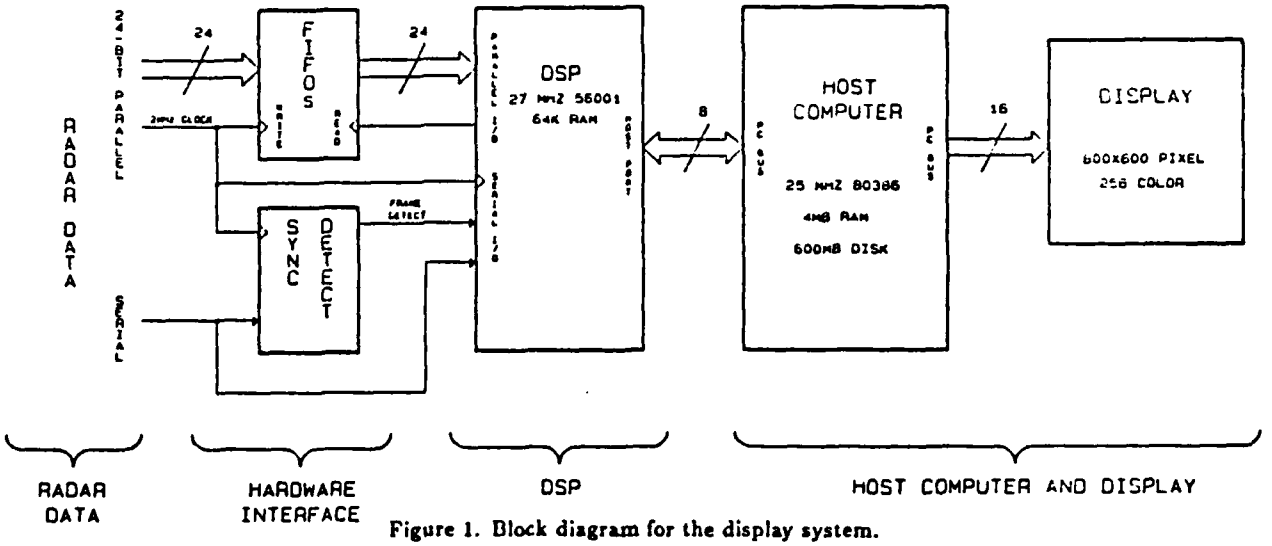

Figure 1. Block diagram for the display system.

30.4

DUAL-POLARIZATION RADAR OBSERVATIONS OF LIGHTNING ECHOES AND PRECIPITATION ALIGNMENT AT 3 CM WAVELENGTH.

Paul R. Krehbiel, William Rison, Steve McCrary, Thomas Blackman, and Marx Brook

Langmuir Laboratory, Geophysical Research Center,
New Mexico Tech, Socorro, NM 87801

Polarization-diverse radar observations provide additional information about the precipitation in a storm, but also enable or enhance one's ability to detect and study other storm phenomena. In this paper we describe results in which 3-cm dual-polarization radar measurements have been used to detect manifestations of the electrical activity in a storm - in particular, to detect lightning echoes at short wavelengths and to detect the presence of electrically aligned particles.

Radar echoes from lightning are commonly detected at wavelengths longer than about 5 cm but have rarely been observed at shorter wavelengths ($\lambda \leq 3$ cm). This leads to the question (Williams et al. 1989) whether the lightning channels are underdense at the shorter wavelengths or whether the echoes are simply masked by stronger precipitation echoes. The former would have implications concerning channel electron densities and temperatures while the latter would have implications concerning the electrification processes in a storm.

The detection of electrically aligned particles is of interest because of the possibility for remotely sensing the local electric field or the presence of electrified conditions inside a storm. Electrical alignment has been detected by Hendry and McCormick (1976) from observations of circular polarization returns at 2 cm wavelength, and inferred by Cox and Arnold (1979) from the depolarization of satellite-earth signals. In both instances the particles appeared to be ice crystals and the alignment exhibited sudden changes that were attributed to the occurrence of lightning discharges within the storm.

The measurements of this paper were obtained using linearly-polarized H and V transmissions that alternated from pulse to pulse. The co- and cross-polar returns were received simultaneously in linear (square law) receivers. The attenuation values of the channels were changeable from pulse to pulse to obtain optimum dynamic range. Although the radar is capable also of alternating between coherent single frequency and incoherent noise transmissions, for the measurements of this study the radar transmitted only broadband (300 MHz bandwidth) noise. The noise transmissions enable the clutter fluctuations from precipitation to be substantially reduced (Krehbiel et al. 1979), which improves the ability of the radar to detect transient events.

Figure 1 illustrates the ability of noise transmissions to reduce clutter fluctuations. Shown is the received power vs. range and time in a fixed direction through precipitation. Standard single frequency transmissions produce the noisy clutter returns of Figure 1a; the 300 MHz noise transmissions produce the steadier returns of Figure 1b. For both transmissions the returns are averaged in range for a time equal to the transmitted pulse length (1 μs).

Figure 2 shows the cross-polar reflected power vs. range and time from a lightning discharge that passed through the (fixed) beam of the radar. The echo lasted about 500 ms and peaked in a single range gate, 22 km from the radar. The narrowness of the echo suggests that it was from a single channel of the discharge. The echo was most prominent in the cross-polar channel due to the decreased attenuation of the receiver for cross-polar returns. Figure 3 shows the simultaneous co- and cross-polar returns and their variation with time. The co-polar return was attenuated by 24 dB relative to the cross-polar return because of precipitation echoes at other ranges. Taking this into account, the cross-polar return was 15-18 dB weaker than the co-polar return.

Figure 4 shows how the lightning echo was correlated with the electrostatic field change of the lightning. (In both this and the earlier figure, the time index is in units of 0.5 ms, corresponding to half the 4 kHz pulse repetition frequency of the radar. The electric field was sampled at the radar prf and was recorded as part of the serial housekeeping data of the radar for good time correlation.) In addition to confirming the lightning nature of the echo, the observations show that the echo began at the same time (within one sample interval) as the electric field change. The long-duration echo at the beginning of the discharge was accompanied by a large initial electric field change, and indicates continuous excitation or current flow along the channel which gradually decreased with time. The impulsive echoes during the final stage of the discharge were associated with step-like electric field changes known as 'k-events'. From optical and photographic observations these are known to produce a transient, high-current discharge along the channel similar to return strokes of cloud-to-ground discharges. The rapid decay of the echo for these events indicates that the channel cools rapidly (in a few ms or less) to an underdense state. The intrinsic cooling rate may be faster than this, as the actual cooling may have been limited by the rate of current decay in the channel.

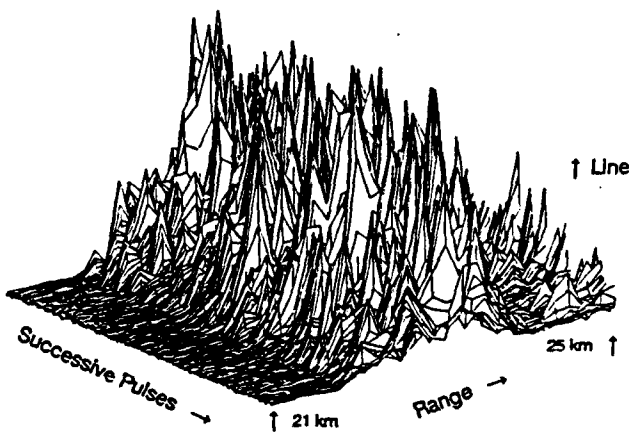

Figure 1a.

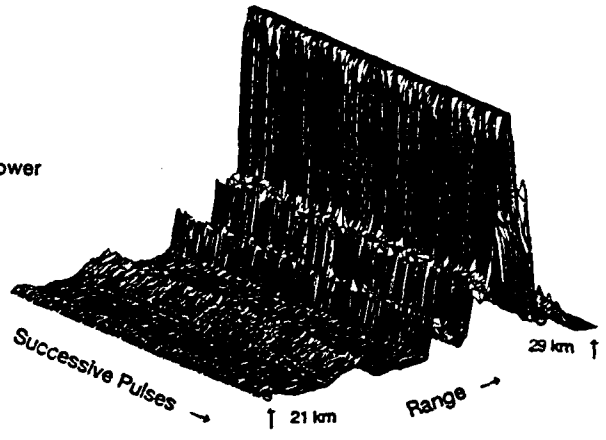

Figure 1b.

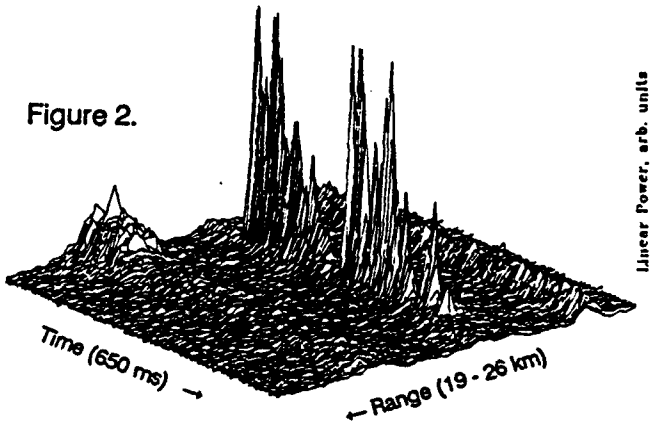

Figure 2.

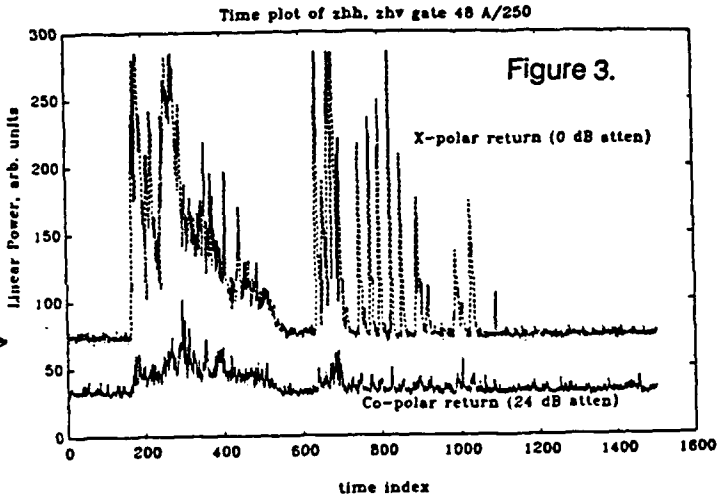

Figure 3.

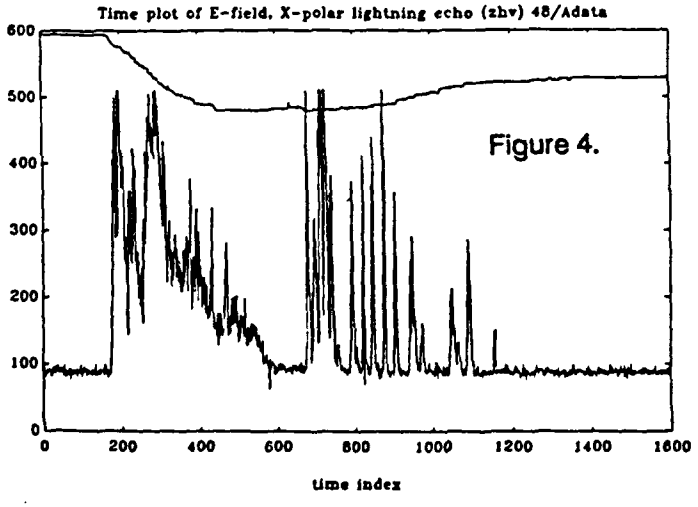

Figure 4.

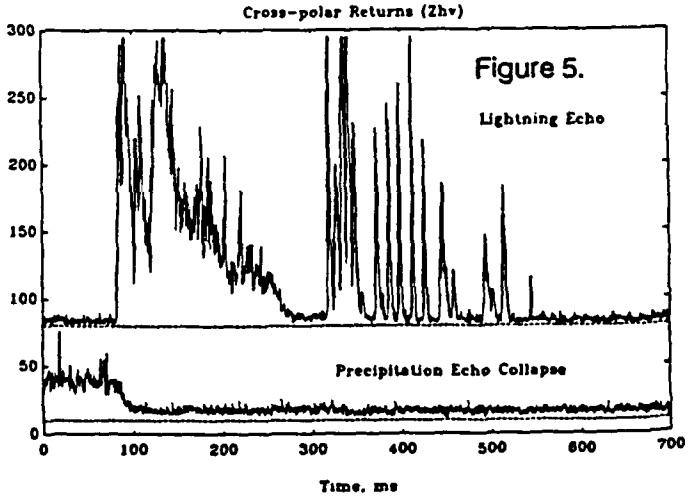

Figure 5.

In addition to the lightning echo, the Figure 2 data also shows the cross-polar return from a precipitation echo, which disappears at the time of the echo. Figure 5 shows the time variation of this return and its correlation with the lightning echo. The precipitation echo collapsed within about 10 ms of the start of the lightning, to below the noise level of the receiver. This indicates that the particles were aligned prior to the discharge, and became de-aligned when the lightning discharge reduced the electric field in the region of the return.

Figure 6 presents 4.5 minutes of observations of the above precipitation echo. During this time, the radar was pointed in a fixed direction 20.5 degrees above the horizon through the upper part of a small, electrically active storm at about 20 km distance. The precipitation echo in question showed up as a localized region of cross-polar return at 24 km slant range on the far side of the storm. The echo was observed in real time on the A-scope of the radar to repeatedly grow and collapse, with the collapses being coincident with the audio output of an optical lightning detector, and often with cross-polar lightning echoes at slightly closer range. This behavior is documented in the figure, which also shows the electric field changes produced by lightning within the storm.

For the first 2 minutes of the Figure 6 data, the cross-polar return exhibited a sawtooth behavior similar to the expected variation of the local electric field in the storm. The cross-polar return would have this time variation if elongated particles were becoming aligned by the local electric field at a non-zero or non-normal angle relative to to the polarization vector of the radar. The co-polar return was attenuated by a constant 24 dB relative to the cross-polar return, and changed only slightly and slowly with time. (The small step changes in the co-polar return were caused by single-gate adjustments of the range gate at which the return was sampled.) Detailed comparison with the electric field change record shows that the echo collapses were associated with small negative field changes; these are known to be due to intracloud lightning in the upper part of the cloud. No cross-polar change (or only a minor change) was associated with the larger positive field changes, which were produced by cloud-to-ground discharges. This is consistent with the fact that CG discharges extend only up to mid-levels in the storm and would be expected to produce a smaller field change in the storm top than IC discharges. (Some field changes were produced by lightning in another storm at a greater distance.)

During the final 2.5 minutes of the record the cross-polar return undulated around a lower value and several lightning events caused the return actually to *increase*. (Two increases also occurred during the first part of the record.) Cross-polar increases can be explained two ways - either the electric field (and therefore the degree of alignment) was stronger after the discharge than before, or the electric field remained strong but changed direction as a result of the lightning. Although the first interpretation is possible, we favor the second interpretation as being consistent with the cross-polar signal between lightning events. In this interpretation, the electric field became approximately aligned with the radar polarization vector (or normal to it), resulting in a minimum cross-polar return which would be sensitive to changes in the alignment direction.

The linear depolarization ratio (LDR) of the aligned particles is somewhat uncertain because of the co-polar attenuation, but appeared to be 3 to 6 dB greater than -24 dB, and varied by a factor of two (3 dB) as the particle alignment changed. Because of their altitude (10.5 km MSL), the particles undoubtedly were ice-form. Other echoes at closer range in the storm had LDR's 6 dB less than -24 dB and did not noticeably change with the occurrence of lightning.

Recent observations (not shown here) at lower altitude above the brightband of a dissipating storm have shown that lightning-associated cross-polar changes occur

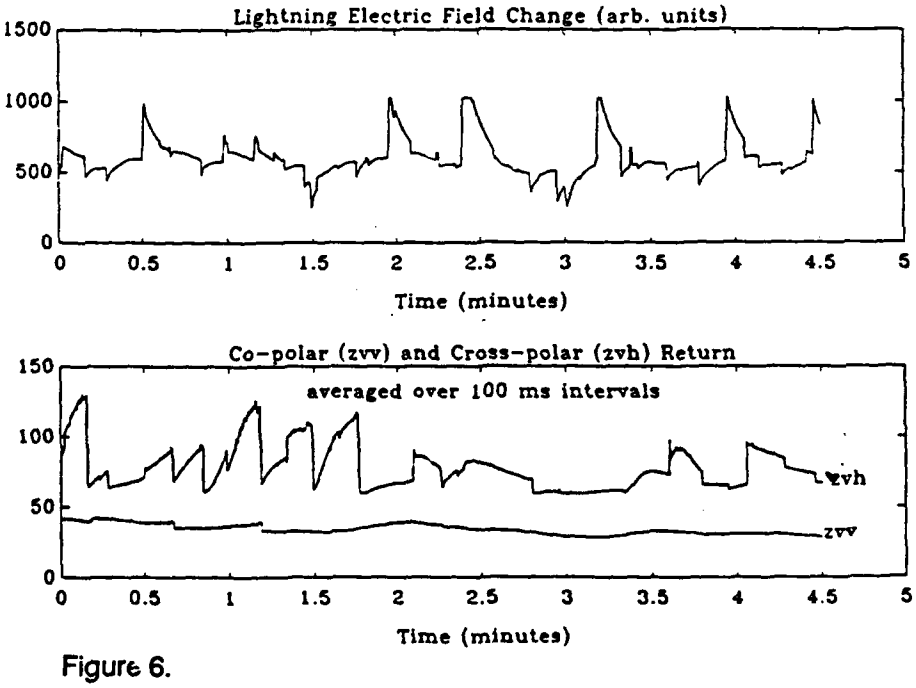

Figure 6.

throughout the horizontal extent of the storm, and indicate that particles commonly become aligned over extensive regions of dissipating storms.

The above observations detect particle alignment using incoherent measurements; of interest in continued studies are coherent measurements, since the co- and cross-polar returns of aligned particles are expected to be correlated. Correlation measurements were used by Hendry and McCormick (1976) to detect alignment and should provide an unambiguous indication of alignment before or in the absence of lightning. Hendry and McCormick also used circular polarization, which they noted would enable the direction of alignment to be ascertained.

In conclusion we return to the lightning echo results. Figure 7 shows volume reflectivity measurements reported by Williams et al. (1989) at longer wavelengths, vs. the observation wavelength. Added to their figure are the apparent (co-polar) volume reflectivities (η) of two representative lightning echoes from the current study. Both co-polar echoes would have been well-masked by 30 dBZ precipitation, or by the normal clutter fluctuations of weaker precipitation. Assuming that the reflectivity values are generally representative of lightning, the lack of observations of lightning echoes at 3 cm wavelength (in comparison with longer wavelengths) implies that the in-cloud portions of discharges tend to be confined to regions of at least mildly reflecting precipitation. A final comment concerns the wavelength dependence of the lightning reflectivity. The dependence is not well understood; the above results suggest that η is approximately constant between 3 and 10 cm wavelength. Additional observations are needed to test these results.

REFERENCES.

Cox, D.C., and H.W. Arnold, 1979: Observations of rapid changes in the orientation and degree of alignment of ice particles along an earth-space radio propagation path. *J. Geophys. Res., 84*, 5003-5010.

Hendry, A., and G.C. McCormick, 1976: Radar observations of the alignment of precipitation particles by electrostatic fields in thunderstorms. *J. Geophys. Res., 81*, 5353-5357.

Krehbiel, P.R., and M. Brook, 1979: A broadband noise technique for fast-scanning radar observations of clouds and clutter targets. *IEEE Trans. Geosci. Elect., GE-17*, 196-204.

Williams, E.R., S.G. Geotis, and A.B. Bhattacharya, 1989: A radar study of the plasma and geometry of lightning. *J. Atmos. Sci., 46*, 1173-1185.

Figure 7.